BINARY–SINGLE STAR SCATTERING. I. NUMERICAL EXPERIMENTS FOR EQUAL MASSES

Piet Hut and John N. Bahcall
Institute for Advanced Study
Received 1982 July 19; accepted 1982 October 18

ABSTRACT

This is the first paper in a long-term project to study gravitational scattering. More than a million numerical orbit calculations have been carried out for binary–single star scattering in the case of equal masses. For the first time a Monte Carlo sampling has been possible over the full dimensionality of phase space without having to make any assumptions about dependence on orientation, phase angles, or impact parameter.

Total cross sections are obtained for ionization, exchange, and resonance scattering, and their detailed dependence on incoming velocity is plotted for initial binary orbits of zero, moderate, and extreme eccentricity. The process of averaging over impact parameter, impact orientation angle, impact direction angles, and binary orbital phase angle produces total cross section curves which are smooth functions of incoming velocity.

Differential cross sections for energy exchange between binary and single star are plotted as a function of energy exchange for several combinations of incoming velocity and binary orbital eccentricity. The relative contributions of flyby and exchange scattering are exhibited separately.

Ionization cross sections are fitted to obtain a simple expression for the dependence on single star incoming velocity and binary eccentricity. The resulting expression is integrated analytically over a Maxwellian spectrum of field star velocities. The thermally averaged ionization rates thus derived are found to be only weakly dependent on initial binary eccentricity over the whole range of thermal velocity dispersions.

All results are in good agreement with analytical approximations by Heggie and by Hut.

Subject headings: stars: binaries — stars: stellar dynamics

I. INTRODUCTION

a) Different Types of Gravitational Scattering

Most *N*-body studies have been performed with an initial distribution of single stars. In the course of the calculations a few binaries generally form dynamically, especially in simulations of dense areas such as the cores of strongly condensed self-gravitating systems, but most stars remain single. However, in the Galaxy the observations show a different picture (Batten 1973): most stars are members of a binary or higher order system. This multiplicity must be a characteristic of the process of star formation, since a thermal equilibrium distribution would imply a much lower abundance of binaries (Heggie 1975*a*). Therefore it seems natural to consider *N*-body systems that consist from the outset of comparable populations of different multiplicities: single stars and binary systems.

With the exception of very close encounters (to within a few stellar radii), star-star scattering is an elastic process. However, binary-star and binary-binary scattering is inelastic. In the latter case energy is exchanged between the relative motion of the centers of mass of the objects and the internal orbital motions of the binaries. Thus if binaries are considered as elementary units, inelasticity becomes a qualitatively new aspect of particle-particle scattering.

The most general treatment would include as particles single stars, binaries, triple systems, etc., and would describe the characteristics of *n*-particle scattering (*n* = 2, 3, ...) for every combination of different types of particles. However, not all cases are equally important, although their relative importance is easy to estimate.

First of all, the importance of triple and higher order systems as a special class is often rather small. The reason is that they are generally unstable toward decay into lower order systems, unless they are built in a hierarchical fashion. In the latter case they behave dynamically as almost independent combinations of lower order systems, albeit with different length scales. An example of a stable hierarchical three-body system is the Sun-Earth-Moon system. Here the internal motions can be described rather well as a simple superposition of two binaries with length scales of 10^{11} and 10^{13} cm.

Second, the importance of two-particle scattering is nearly always much greater than that of three-particle scattering, simply because the former is proportional to the particle density squared whereas the latter is proportional to the cube of the density. Only in very dense regions is this no longer true.

The above considerations naturally lead to the study of binary–single star scattering and binary-binary scattering, as the two dominant inelastic processes of

319

interest in realistic star systems. A detailed knowledge of these two processes is the aim of our study and hopefully will make possible more realistic N-body simulations using binaries as well as single stars as basic units.

There are exceptional cases for which star densities are so high that physical collisions are significant, and encounters to within a few stellar radii make possible the dissipation of energy via excitation of eigenmodes in the stars (Fabian, Pringle, and Rees 1975; Press and Teukolsky 1977). Inclusion of these processes would require many more parameters because tidal dissipation is strongly dependent on the particular type of stars that are involved and their spectrum of eigenmodes (Zahn 1977). Moreover, the scale independence of Newton's law of gravity for point particles, which allows scaling of masses and distances for a fixed value of the gravitational constant, is broken upon introduction of particular stellar models. Therefore we will treat all stars as point particles, which is a relatively accurate approximation in many astrophysical applications.

b) Previous Work

The best general reference for the theory of binary–single star scattering is the detailed study by Heggie (1975a), in which many earlier references, as well as much outstanding original work, can be found. For shorter introductions and reviews we refer to Heggie (1975b, 1977, 1980). Later references for the specific study of resonance scattering are Monaghan (1976a, b, 1977) and Nash and Monaghan (1978).

On the experimental side, several extensive series of numerical orbit calculations have appeared. Among these we mention Hills (1975), Hills and Fullerton (1980), Fullerton and Hills (1982); and Saslaw, Valtonen, and Aarseth (1974), Valtonen and Aarseth (1977), Valtonen and Heggie (1979). Earlier, less extensive calculations are referred to in the above papers. Most of these studies have necessarily been limited (see below) to specific choices for the dependence of the cross sections on particular parameters or to a restricted sampling of parameter space.

The difference between classical gravitational scattering, discussed here, and quantum mechanical scattering, as studied in atomic and elementary particle physics, is important. For a change, the quantum mechanical treatment is easier in many ways, since the lower lying energy states of simple systems often show a large spatial symmetry. Therefore only a few relevant variables have to be taken into account in the treatment of scattering processes. On the other hand, even the simplest case of classical binary–single star scattering requires the full treatment of nine independent parameters, which cannot be reduced by further rescaling or coordinate choices, as will be discussed in the next section. The second simplest case, binary-binary scattering, requires an irreducible set of 16 parameters. In both cases the outcome of a single scattering experiment is extremely sensitive to many parameters such as phase and orientation angles. It will be clear that Monte Carlo methods are necessary here in order to arrive at averaged probabilities in the form of cross sections.

There are, however, several parallels between atomic physics and stellar dynamics. Basic processes such as ionization, resonance scattering, and charge exchange find their obvious counterparts in gravitational scattering. Besides, for higher energy levels the quantum treatment of atomic processes goes over asymptotically into a classical treatment, according to the correspondence principle. This is the reason that several studies have appeared of the classical theory of atomic scattering, together with numerical orbit calculations similar to the gravitational ones mentioned above. Three references, Percival and Richards (1975), Olson and Salop (1977), and Shakeshaft and Spruch (1979), may form a useful introduction to classical atomic scattering.

Of course, apart from quantum mechanics there are still major differences between scattering in classical electrodynamics and in Newtonian gravity: neutral atoms exert only tidal forces on charged particles outside their immediate vicinity, whereas binaries always exert a long range force from their center of mass; charge and mass are unrelated in electricity whereas gravitational and inertial mass is the same in gravity; and no fixed mass ratios are known to occur in stellar dynamics whereas in atomic physics the electron-proton mass ratio is a natural constant.

We adopt here the terminology of atomic physics in describing the results of our numerical experiments for stellar scattering experiments.

c) Outline of the Project

We give in this paper a first report of an extensive project that is designed to provide a representative coverage of binary–single star scattering, and at least an exploration of binary-binary scattering. Our aim is to present cross sections and reaction rates that are obtained by numerical orbit integration from initial conditions determined by Monte Carlo techniques. The main difference from the previous work mentioned above is the large amount of computer time available, which has already made possible the more than a million orbit calculations analyzed in the present paper. All calculations described here have been performed by a fully automatic program which was put into operation soon after the Institute for Advanced Studies acquired a Vax 11/780. This program runs in a background mode and effectively soaks up all otherwise unused computer time (about 2 months' worth of computing time for the calculation of the data described in this first report).

The data available from our calculations are more than a order of magnitude more extensive than the total of all previously published computations. This makes possible qualitative as well as quantitative improvement in the analysis of the numerical experiments. It is now possible, for the first time, to explore all nine irreducible parameters of the gravitational scattering process simultaneously to obtain fully general and realistic results. Previously published results have been obtained using restrictive assumptions,

which were designed either to test specific hypotheses and approximations, or to extrapolate from a limited sample to more general situations (e.g., parabolic encounters in Saslaw, Valtonen, and Aarseth 1974, and zero impact parameter in Hills 1975, Hills and Fullerton 1980, and Fullerton and Hills 1982).

The present paper explores the case where all three stars have equal masses, for high and intermediate energy of the field star incident on the binary. The rather separate case of low field star energies ("hard" binaries, where resonance scattering is important) will be treated in subsequent papers. Other mass ratios will also be treated in the future, both for different single-star masses and for unequal masses of the binary members themselves. Preliminary calculations for all of these problems have already been carried out, and programs are currently running on the IAS Vax to generalize the results of the present paper to different mass ratios.

d) Outline of this Paper

In the first half of the present paper we describe a framework of binary-single star scattering, for the most general case. In the rest of the paper data are presented for the case where all stars have equal masses. Although this is a special situation, it is of practical interest for applications in simple astrophysical models; many of the N-body simulations that are currently studied assume equal-mass particles. Also some of the results obtained here for the equal-mass case are valid, with only slight generalizations, to the case of unequal masses. Results for other mass ratios will be presented in future publications.

In § II we describe the setup of the individual scattering experiments. Starting from 22 coordinates and parameters, we arrive at an irreducible set of nine. For each of these we discuss the range and weight functions for sampling the initial values in Monte Carlo fashion. We also describe the numerical integration scheme, and the automatic method to halt integration after scattering has reached the asymptotic regime.

In § III the analysis of a complete series of scattering experiments is outlined and the reduction of the data to obtain total and differential cross sections is described. Statistical and systematic errors are evaluated. A series of test runs is described in which some parameters have been chosen on a grid while other parameters were held fixed.

In § IV the main results are presented in the form of cross sections for circular, as well as moderately and extremely eccentric, binary orbits. Total cross sections are given for ionization, exchange, and resonance scattering. For soft binaries also differential cross sections are presented for arbitrary values of energy exchange between the binary and the field star. Differential cross sections and other, more detailed information for hard binaries, where resonance scattering is possible, will be given in a future publication.

In § V the ionization cross sections are averaged over a thermal spectrum of field star energies to obtain an expression for the thermal ionization rate as a function of binary eccentricity and field star velocity dispersion. Finally, § VI presents a discussion of the main results.

II. INDIVIDUAL SCATTERING EXPERIMENTS

a) Coordinates and Parameters

The dynamics of the three-body problem is governed by the system of nine coupled, second-order, nonlinear differential equations:

$$\ddot{r}_i = -G \sum_{i \neq j} \frac{m_j(r_i - r_j)}{|r_i - r_j|^3} . \qquad (2.1)$$

In general the evolution of the system is determined for $-\infty < t < +\infty$ after the specification of 18 initial conditions $r_i(0)$, $\dot{r}_i(0)$ and the four constant parameters G, m_i. The exceptional set of initial conditions for which collisions occur is negligible (it forms a finite collection of submanifolds of dimensionality 2 lower, and therefore a set of measure zero, whereas the set which results in triple collisions has in total five dimensions less; Siegel and Moser 1971).

We are interested in the solutions to equation (2.1) which correspond to scattering of a single star incident on a binary. For $t \to -\infty$ the motion then decouples into two two-body motions. If the total energy is positive, the stars cannot form a bound triple system and for $t \to +\infty$ the system again decouples, either in three single unbound stars or in a single star escaping from a binary. If the total energy is negative, a bound triple system might form temporarily but will in general dissolve in some 10 or 100 crossing times (Valtonen and Aarseth 1977). In any case, for negative total energy the system will ultimately decouple into a binary and a single star (with exceptions to this rule again forming a set of measure zero; see Alekseev 1981 for a clear review of qualitative methods in modern topology and its applications to the three-body problem).

In the whole of three-body phase space we can discern four distinct asymptotic regions in which genuine three-body interaction is negligible: one in which all three stars are unbound, and three in which one pair of stars is bound and the third star is unbound. Scattering experiments define a mapping from the union of these asymptotic regions of three-body phase space in itself, orbit into orbit; or equivalently of surfaces of section transverse to those orbits, point into point.

To borrow a picture of Alekseev (1981), these orbit families can be visualized as rivers streaming from the asymptotic regions into a central interaction area, where they show a fantastically complicated pattern of branching. Depending on the precise location of watersheds, each little stream then flows into larger rivers, ultimately to collect in a major river connecting again to one of the four asymptotic regions. Although the asymptotic description is simple, the microscopic flow in the interaction area is of such complexity that nearby initial conditions in one asymptotic region often lead to final positions in different asymptotic regions. This is the main reason one must use Monte Carlo methods to

determine the average width of the main channels in three-body phase space.

From the 18 coordinates of the initial conditions, only nine determine different patterns of this mapping; the others add shifts and rotations of the pattern as a whole. This follows from the six degrees of freedom in the choice of position and velocity of the center of mass, and the three degrees of freedom in the orientation of the coordinate system in which the mapping is to be described. A convenient choice to suppress these degrees of freedom is to choose the center of mass of the original binary at rest at the origin, and the binary orbit in the (x, y)-plane with the periastron of the second star on the positive side of the x-axis (see Fig. 1).

The remaining nine initial coordinates and four parameters can be further reduced by scale transformations in the physical dimensions of length, time, and mass. Again the pattern of the mapping remains invariant under these linear transformations, which merely map different physical systems into the same mathematical model. A convenient choice is to set the semimajor axis, the sum of the masses of the original binary, and the gravitational constant all equal to unity.

We are now left with eight initial coordinates and two parameters, which determine the subsequent evolution. However, they are still not all unique: the same set of orbits can originate from different initial conditions, which one imposed at different positions in the orbits. A practical choice is to fix the initial separation of the field star from the center of mass of the binary at a constant value. In most of our calculations, we used an initial distance of 20, measured in units of the semimajor axis of the binary.

The mapping between IN and OUT states of a field star scattering off a binary can be completely studied in a nine-dimensional space of initial values. The nine variables parameterizing this space can be any independent combination of the original four parameters and 18 coordinates in the three-body phase space. Our parameterization, after having made the above choices of conventions, is summarized in Table 1 and is illustrated in Figure 1.

TABLE 1

PARAMETERIZATION OF INITIAL VALUES FOR SCATTERING OF A
SINGLE STAR OFF A BINARY

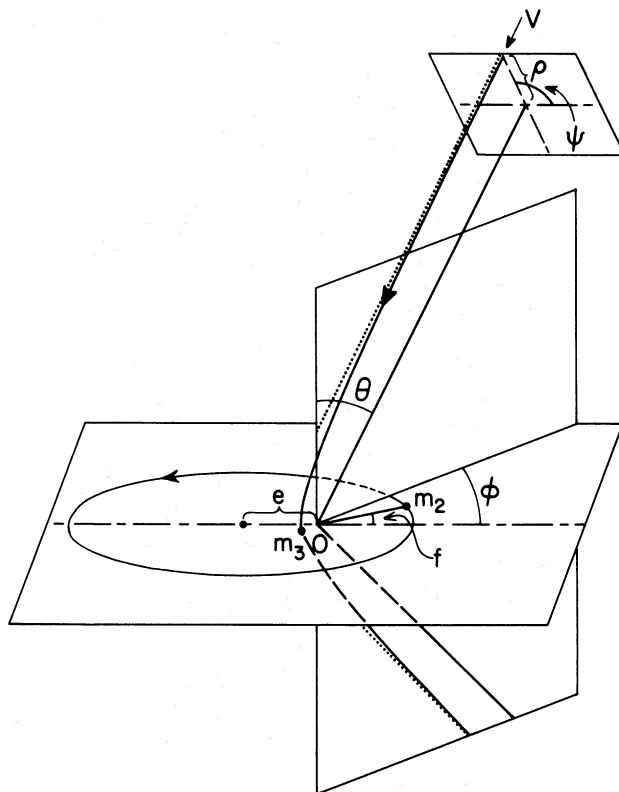| Variable	Range	Description
m_2	$[0, 0.5]$	Mass of lightest binary member
m_3	$[0, \infty)$	Mass of field star
e	$[0, 1)$	Initial eccentricity of binary
v	$(0, \infty)$	Asymptotic incoming velocity of field star with respect to center of mass of binary
ρ	$[0, \infty)$	Impact parameter
φ	$[0, 2\pi)$	Impact direction
ϑ	$[0, \pi/2]$	Impact direction
ψ	$[0, 2\pi)$	Impact orientation
f	$[0, 2\pi)$	Projected true anomaly of the binary at the time that the incoming field star would have reached its hyperbolic pericenter

FIG. 1.—Unperturbed two-body orbits illustrate the parameterization of initial values for scattering of a field star off a binary. The nine independent variables are defined in Table 1. The elliptic orbit describes the motion of the lightest binary member in the absence of the field star. The hyperbolic orbit describes the motion of the field star with respect to the center of mass 0 of the binary in the limit of negligible binary separation. Although poor approximations to the real orbits, they form a convenient reference frame to define the initial values in a coordinate independent way. An example is the definition of the binary phase angle, f, as the angle with respect to periastron which the lightest member of the binary would have at the time of pericenter passage of the field star in these unperturbed orbits.

b) Numerical Integration

A scattering problem is defined as a mapping from the state of the whole system from $t \to -\infty$ to $t \to +\infty$. To determine this mapping, the evolution of the system has to be computed. Except for a short period of appreciable three-body interaction, this can be done analytically in a two-body approximation. Figure 2 illustrates how the numerical calculation starts at a fixed distance before closest encounter (typically 20 times the binary semimajor axis) at the point corresponding to the unperturbed hyperbolic motion. The parameters describing the hyperbola are themselves derived from the one-body approximation of a straight line: the impact parameter d and the asymptotic velocity v_∞.

A fourth order Runge-Kutta scheme was used for the numerical integration of equation (2.1). It has the advantages of being simple, self-starting, and allowing frequent changes of step size without additional
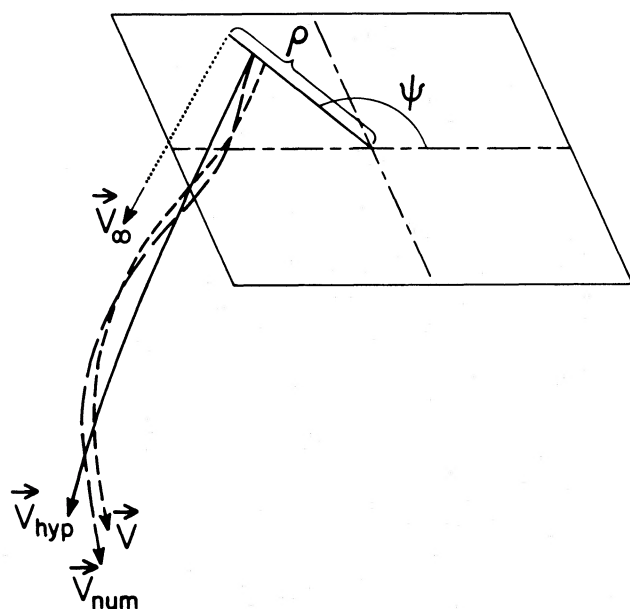
FIG. 2.—The real orbit of the incoming star (*short dashes*) compared to the one-body approximation of a straight line (*dotted line*) to determine the impact parameter, the two-body approximation of a hyperbola (*full line*), and the numerically computed orbit (*long dashes*). Final accuracy is determined by a combination of the error in initial position and errors in the numerical integration. Initial values ρ, ψ, v_∞ as in Fig. 1.

computation. The step size was determined with every new integration step as

$$dt = \epsilon \min_{\{i,j\}} \frac{|r_i - r_j|}{|v_i - v_j|} \qquad (2.2)$$

where ϵ is a constant, a typical value being $\epsilon = 0.1$. Although both potential and kinetic energy can become arbitrarily large during a close passage of two stars, the above prescription is a simple regularization whereby no pair of stars can undergo a large change in one step.

It is not possible to provide a fixed value of ϵ in order to stay within a desired numerical accuracy. The reason is that the number of integration steps varies enormously from orbit to orbit. Therefore orbits with a very close encounter or a temporarily bound triple system require a much higher accuracy per integration step. Unfortunately, at the outset of the calculation it is not known what kind of orbits will result.

This problem was avoided by starting every computation with a fixed value of ϵ, typically $\epsilon = 0.2$. Checks of numerical errors were made by regularly calculating the total energy, which is a conserved quantity. Whenever the total change in energy exceeded a limit, the integration was halted and started all over again with ϵ twice as small. Throughout we used 1% of the binding energy of the original binary as our limit of tolerance. Because we used a fourth order integration scheme, the error per time step was reduced by a factor of about 32 in each new iteration. Thus only in very few cases ($\ll 1\%$) did more than one rerun have to be made.

c) Initial Conditions

To arrive at a complete understanding of gravitational binary scattering we have to compute orbits for general values of each of the nine parameters specifying the initial state, as derived in § IIa. If we used 10 sampling values for each parameter, we would have to compute 10^9 different combinations of orbits. This would take 100 years with the Vax 11/780 we used. Even then, the resolution in parameter space would be rather coarse, and, what is worse, important resonance peaks in the angle dependence of the cross section might be overlooked.

In geometrical terms, the cross section for a certain process to happen is proportional to the volume in the space of parameters occupied by initial conditions leading to the outcome of interest. The most efficient way to integrate a volume with a complicated contour in a space of high dimensionality is to use the Monte Carlo method. The simplest version of this technique is a random hit-or-miss search homogeneously spread out over that fraction of parameter space where a certain outcome is allowed by conservation laws. In this case the relative error in a cross section for a certain process is inversely proportional to the square root of the number of times that the outcome is observed.

More sophisticated versions of Monte Carlo calculations are in use for cases where the contours of the regions to be integrated are relatively smooth and some *a priori* knowledge of their position is available. In the present case these techniques are not applicable, because of the very complicated dependence of the outcome of a scattering experiment on the four initial angles, which creates bizarre contours in parameter space.

The advantages of a Monte Carlo method over a direct grid search are thus twofold: a good impression of cross sections can be obtained with a much smaller number of computed orbits, and it is very simple to estimate the uncertainty.

In the simple Monte Carlo approach of uncorrelated determinations of initial conditions, three decisions have to be made for every parameter before a complete series of computations is started. First of all, the range of permitted values has to be specified. Second, because some parameter regions have a higher probability to occur, one should also specify which combination of parameters should be given equal probability to occur. Finally there are different sampling techniques. One can start every new experiment with the full range for a certain parameter to be chosen from, resulting in a maximally random sampling. Or one may divide the full range in smaller intervals from which one chooses initial conditions subsequently. This latter, layered sampling guarantees a better coverage of the whole parameter domain, without introducing extra bias. In Table 2 a convenient choice is given for the nine parameters defined in Table 1.

To start with column (2), choosing fixed values for the mass ratios and the binary eccentricity constitutes a major simplification. It is justified because there is no

TABLE 2

Determination of Initial Conditions in Monte Carlo Fashion

Variable (1)	Range (2)	Probability Homogeneous in (3)	Sampling Method (4)
m_2	constant	...	fixed
m_3	constant	...	fixed
e	constant	...	fixed
v	(v_{min}, v_{max})	v	layered
ρ	$[0, \rho_{max})$	ρ^2	layered
φ	$[0, 2\pi)$	φ	random
ϑ	$[0, \pi/2)$	$\cos \vartheta$	random
ψ	$[0, 2\pi)$	ψ	random
f	$[0, 2\pi)$	$E - e \sin E$	random

reason to expect a very strong dependency on each of these values *after* averaging over all other parameters, except possibly around the degenerate case of equal masses. But this last case is interesting in itself because it serves as an ideal situation with which to compare analytic calculations and permits the simplest applications in models of astrophysical interest.

After these initial choices it is safer to fix no additional parameters. It might be that, for example, a strong dependence on velocity, for *fixed* eccentricity, could be missed in a grid choice of velocities. Therefore velocity values were sampled over the whole range of interest. Impact parameters were taken between zero and the maximum value for which certain processes of interest would be possible. This value ρ_{max} must be larger for smaller incoming velocity v, due to gravitational focusing, which leads to $\rho_{max} \propto v^{-1}$. It is convenient to use the same functional form of $\rho_{max}(v)$ in different series of experiments, in order to obtain a homogeneous data base.

A simple choice which we have adapted here is

$$\rho_{max}(v) = (C/v + D)a , \qquad (2.3)$$

where a is the semimajor axis of the original binary. We use the notation v for the incoming velocity of the field star with respect to the binary, measured in units of the critical velocity v_c, for which the total energy of the three-body system vanishes. Thus v is dimensionless, and

$$v_c^2 = G \frac{m_1 m_2 (m_1 + m_2 + m_3)}{m_3 (m_1 + m_2)} \frac{1}{a} , \qquad (2.4)$$

where G is the gravitational constant.

The constants C and D have to be chosen appropriately for the process one wants to study. For example, to determine ionization cross sections, $C = 4$ and $D = 0.6(1 + e)$ are appropriate. This choice defines a contour which envelops all initial values leading to ionization, without being wide enough to weaken the statistics. The above values have been found in a series of test runs.

The first term in equation (2.3) describes the gravitational focusing, and dominates for intermediate and low velocities. For very high incoming velocities, the

last term in equation (2.3) dominates. In this regime, only very close encounters have an appreciable effect. Therefore the contour has to be just slightly larger than the maximum separation of the binary members and their center of mass, which for equal masses is $\frac{1}{2}(1 + e)$.

In column (3) of Table 2 the combinations of parameters are given which we sampled with equal probability. For the incoming velocity, no extra weight function was chosen. In applications to determine the rate of several processes in different astrophysical environments, the cross sections must be weighted with, for example, Maxwellian velocity distributions. This weighting depends on the environment of interest, and can be done after the velocity dependence of the cross sections is fitted to a simple parameterization.

The impact parameter is sampled according to an equal probability distribution for ρ^2, the area of a surface element transverse to the direction of the incoming star. This corresponds to a probability weight proportional to ρ. The spherical angle ϑ occurs in the surface element $\sin \vartheta\, d\vartheta d\varphi = d(\cos \vartheta) d\varphi$, and therefore $\cos \vartheta$ is sampled with equal weight. This produces a probability weight for ϑ proportional to $\sin \vartheta$.

The choice of weight functions in Table 2 is especially convenient in that no later corrections are required for computing probability distributions or cross sections.

To obtain the correct probability distribution for the initial phase f in eccentric orbits, care has to be taken to give every angular element a weight equal to the fraction of the time which the system spends in that part of the orbit. No explicit expression can be given for $f(t)$. Instead we have to solve Kepler's equation:

$$\frac{2\pi}{T} t = E - e \sin E , \qquad (2.5)$$

where t is the time since periastron passage, T is the orbital period, and E is the eccentric anomaly, related to the true anomaly f by

$$\tan \left(\frac{f}{2}\right) = \left(\frac{1+e}{1-e}\right)^{1/2} \tan \left(\frac{E}{2}\right) . \qquad (2.6)$$

The phase f can be determined as follows. First a random number is chosen between zero and 2π, as the value of the combination $E - e \sin E$. From this E can be approximated in successive iterations. Care has to be taken to avoid overshooting or instabilities for high eccentricities. Finally equation (2.6) then gives the initial value for f.

The choices of sampling methods, summarized in column (4) of Table 2, give a maximal layering in v and ρ. This minimizes statistical fluctuations in the dependence of the final results on these parameters, which are of most interest. For astrophysical applications, we are not especially interested in angular dependencies. Therefore the four angles are sampled randomly (more layered sampling is unnecessary and would require an even larger number of orbits).

d) Outcome and Data Storage

The outcome of a scattering experiment can take one of three different forms. The first possibility is the escape of one star leaving behind the other two in a bound system. We will call this a *flyby* if the new binary is formed by the same stars which made up the old binary; and an *exchange* if the original field star forms part of the new binary, in analogy with the phenomenon of charge exchange in atomic physics. Both flyby and exchange can occur for any amount of total energy of the whole system.

The second possibility is that all three stars become unbound and escape to infinity in different directions. We call this *ionization*, again using atomic physics terminology. Only for positive total energy can ionization occur.

The third possibility is that the stars form a temporarily bound triple system. This we call *resonance scattering* (as in atomic physics). It can only occur for negative total energy. Strictly speaking, resonance scattering is not a completely different type of outcome, since it results either in flyby or in exchange. Ultimately the bound three-body configuration will decay into an escaping star and a binary, typically in some 10 or 100 crossing times.

However, the dynamics of resonance scattering is sufficiently more complicated to warrant a special analysis. Also, from a practical point of view, to follow the whole evolution of the slowly decaying three-body configuration would take a very large amount of computer time because the outcome is extremely sensitive to slight variations in the initial conditions. Therefore numerical integration was generally halted after a few pulsations of such a configuration, postponing a detailed study of resonance scattering to future publications.

To run many thousand experiments requires a fully automatic test procedure to determine the point at which numerical integration should be halted. This test subroutine must be able to predict when the switch can be made to an analytic two-body approximation, within a given accuracy. It also must recognize which of the three types of outcome outlined above has taken place.

To avoid wasting computing time, a test procedure has been designed which is applied only after the point of closest triple approach. A convenient measure in this respect is the mean square distance

$$s(t) = \left[\frac{1}{3} \sum_{i<j} |r_i(t) - r_j(t)|^2 \right]^{1/2} , \qquad (2.7)$$

which can be small only when all three stars are close together. At the beginning of a numerical integration, $s(t)$ monotonically decreases. After $s(t)$ passes through its first minimum, the test procedure is applied once after every 20 integration steps, as detailed in Appendix A.

At the end of each orbit integration, 38 numbers were stored, to provide a detailed description of initial and final conditions, close approaches, and numerical stability. Only a fraction of the huge data base thus collected has been actually used to obtain the cross sections given in the following sections. However, it seems worthwhile to retain more detailed information, both for future investigations and for consistency checks, notwithstanding the considerable burden of handling hundreds of megabytes of information.

Besides initial and final conditions and the type of outcome, the minimum value of the distance between each pair of stars was recorded, and also the minimum in the mean square distance $s(t)$, to provide information about the occurrence of close triple encounters. The number of sign changes in $ds(t)/dt$ was retained as the number of oscillations in temporarily bound triple systems. To provide diagnostics of the numerical performance, a series of numbers was recorded: the two maximum deviations of total energy in positive as well as in negative direction, the number of reruns with smaller step size, and the total number of integration steps.

Some of the complexity of resonance scattering is illustrated in Figure 3, where the orbits of the three stars are plotted for a particular scattering event. In Figure 3, the field star (number 3) moves from the right at zero impact parameter toward the binary (containing stars 1 and 2), at a relative velocity $v_3 = \frac{1}{5}v_c$. The orbits are displayed in the center of mass frame and therefore the field star moves twice as fast as the binary since all stars have equal masses. After a number of oscillations of the whole system, one of the original binary members (number 2) escapes, leaving behind a newly formed binary (numbers 1 and 3). For simplicity in visual presentation, the trajectory of the incoming star has been chosen to lie in the plane of the original binary, thereby reducing the problem to two dimensions.

To display a more detailed history of the orbits, the total scattering process has been divided in six epochs, in Figures 4a–4f. It is clear that most of the time the orbits can be approximated reasonably well by a superposition of ellipses, describing the motion of the center of mass of a close pair, their relative motion, and the motion of the third star. Only Figure 4d is an exception to this rule. However, the parameters of these near-elliptic motions are determined in fast three-body encounters which are extremely sensitive to changes in initial conditions, making a global analytic analysis prohibitively complicated. This results in an erratic exchange of stars forming temporary binaries: in Figures 4a, 4b, 4c, 4e, and 4f, binaries are formed by the stars numbered (1, 2), (2, 3), (1, 2), (2, 3), and (1, 3), respectively. The reader can easily see from Figures 3 and 4 the impossibility of an accurate *analytic* treatment of this kind of scattering event.

The general three-dimensional case of resonance scattering is qualitatively similar to the two-dimensional example discussed above: during scattering most of the time the three-body system displays a hierarchy where one star moves around in an elongated orbit, with little interaction with the remaining binary. However,
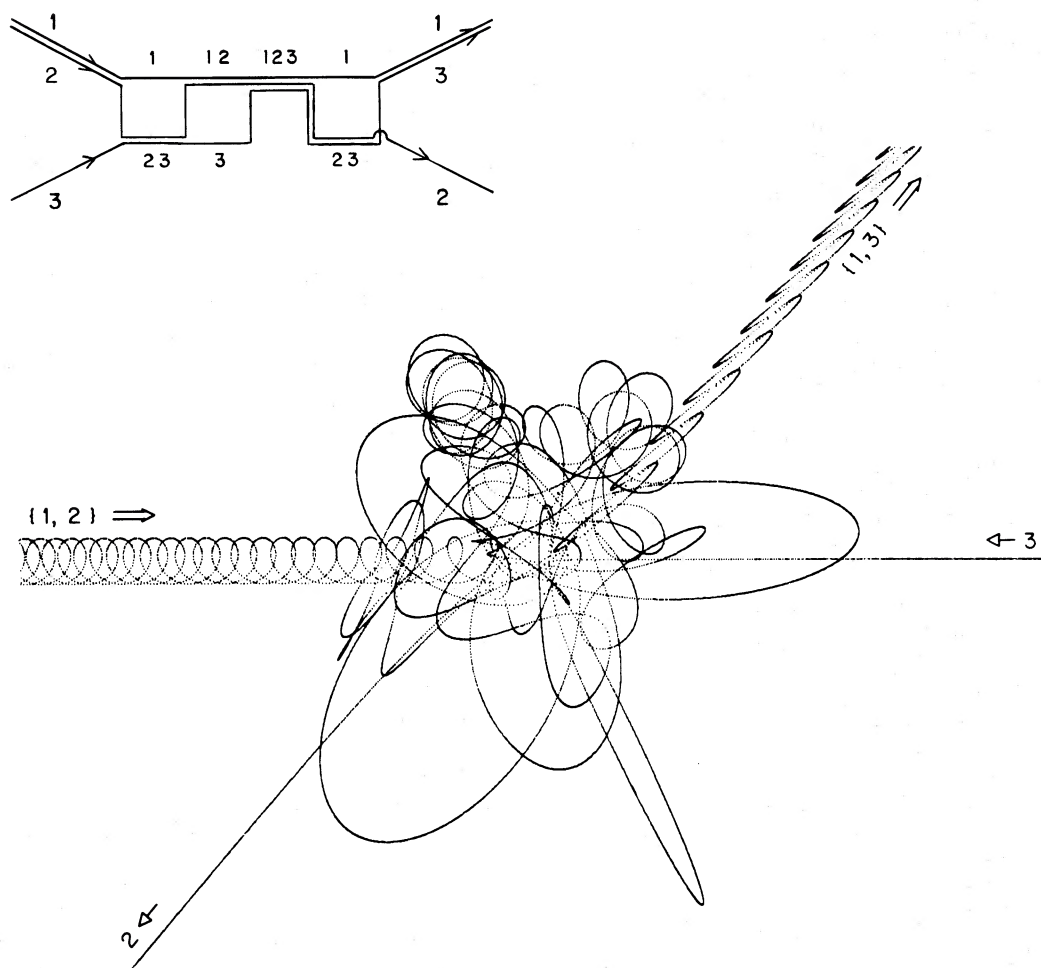
FIG. 3.—An example of a resonance scattering process involving a hard binary and a field star. The trajectories of the three equal-mass stars are plotted in the center-of-mass frame. To help a visual interpretation, the orbits are constrained to two dimensions. However, all features present here are representative for the three-dimensional case as well (the $> 10^6$ orbits reported in this paper are fully 3D). The original binary comes in from the left, and contains the stars that are labeled 1 and 2. The single star comes in from the right and is labeled 3. The orbits are represented by dots spaced at constant time intervals. The outcome of the scattering process is an exchange: star 2 escapes, leaving 1 and 3 behind as a newly formed binary. In the upper left-hand corner the degree of mutual gravitational binding of the three stars is represented schematically in a scattering diagram.

both in two and in three dimensions the general case is even considerably more complicated than the example displayed in Figures 3 and 4 suggests. While Figure 3 displays three phases in which different hierarchies are present, the average number of such excursions is considerably higher, of order 10 or 100. In some of these excursions the stars travel out to much larger separations than those illustrated in Figure 3. A more typical picture of a resonance scattering event looks more like a dense web of orbits around the center, with many spikes sticking out in the form of long and elongated orbits. All this may illustrate why no useful analytic solution of the three-body problem has been found.

III. DETERMINATION OF CROSS SECTIONS

a) Numerical Experiments

In this section we give the main results of the 1.7 million orbit calculations for equal-mass systems. For every series of numerical integrations five numbers had to be specified, as explained in the previous section, equation (2.3). These are the original binary orbital eccentricity e, limits on the range of incoming velocities v_{min} and v_{max}, and the parameters C and D which define a contour limiting the impact parameter ρ.

Most runs were made with the choice $C = 4$ and $D = 0.6(1 + e)$, which defines a domain in parameter space large enough to include all cases ending in
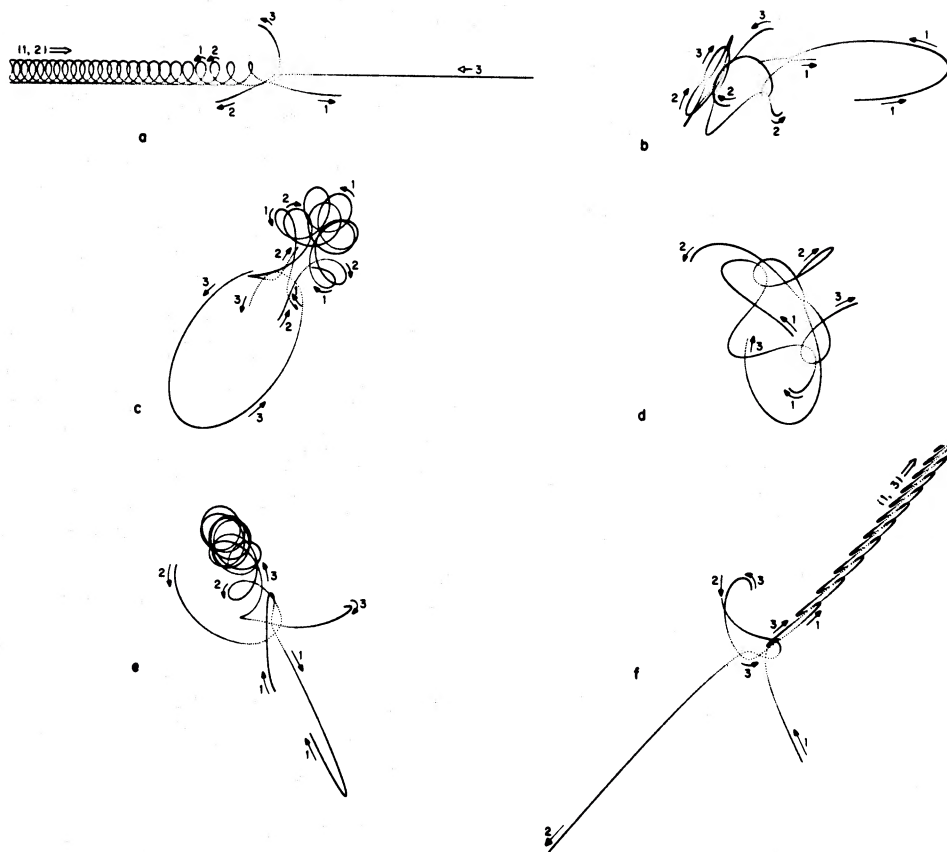
FIG. 4.—The orbits in the resonance scattering process of the previous figure are displayed here in six subsequent epochs, from a to f. In Fig. 4a the first two two-body encounters are shown, first between 1 and 3 followed by that between 1 and 2. In Fig. 4b, 2 and 3 form a short-lived binary, while 1 makes an elliptic excursion. Fig. 4c shows the same process, with 1 and 3 interchanged. In Fig. 4d a period of genuine three-body interaction is displayed, where the individual orbits do not even resemble ellipses. In Fig. 4e, 2 and 3 again form a binary, with 1 traveling off in an elongated ellipse. In Fig. 4f the resonance situation ends: star 2 travels off to infinity with positive energy, leaving 1 and 2 behind as a tight binary.

resonance, exchange, and ionization. The determination of differential cross sections for cases of flyby as a function of the change in the binding energy of the binary requires a wider contour in parameter space. The choice of $C = 8$ turns out to cover all initial conditions leading to an energy change of 10% or more.

The velocity interval used is $(v_{min}, v_{max}) = (\frac{1}{2}, 16)$, expressed in units of v_c, the critical velocity defined in equation (2.4) for which the total energy is zero. This velocity range is divided logarithmically into five subintervals, each of which doubles the velocity of the previous one. Each subinterval is divided linearly into 20 slabs, while a typical 5 hour run enables a stratified sampling of 100 scattering experiments per velocity slab, for different impact parameters.

Nine binary eccentricities were chosen with the following number of orbit integrations for $C = 4(8)$: $500K$ $(200K)$ for $e = 0$; $250K$ $(100K)$ for $e = 7$; and $50K$ $(40K)$ for each of the values $e = 0$, 0.2, 0.4, 0.55, 0.7, 0.8, 0.9, 0.95, 0.99 (here K denotes 1000 numerical experiments). An additional $9K$ orbits were integrated for $e = 0$ and very low incoming velocities in the range

$(v_{min}, v_{max}) = (1/16, 1/2)$, which required an increase in typical integration time per scattering experiment by more than an order of magnitude.

For each orbit integration 38 numbers were stored, as detailed in the previous section, leaving us with a total of more than 6×10^7 numbers. These contain information about the gravitational scattering process as a mapping between IN and OUT states, with a wealth of information about detailed angle dependences, closest pair and triple encounters, etc. In order to summarize the overall probability of certain outcomes of special interest, we present them in the form of cross sections defined below.

b) Cross Sections

The cross section σ_X for the outcome of a scattering experiment to have the characteristic X (e.g., ionization) is determined as follows. For a given eccentricity e and incoming velocity v, there generally exists an upper limit $\rho_{max}(v, e)$ on the impact parameter ρ, above which no outcome of type X is possible, since the three-body

interaction becomes arbitrarily small for very large ρ, at least for *fixed* e and v.

Since classical mechanics is fully deterministic, the probability $p_X(\varphi,\ \vartheta,\ \psi,\ f;\ \rho,\ v,\ e)$ that the outcome of a scattering experiment is of type X for a complete set of given initial conditions, is either zero or one. The averaged probability to obtain X, when no *a priori* information on the four angles is available, is given by

$$P_X(\rho, v, e)$$

$$= \frac{1}{8\pi^3}\frac{1}{P}\int_0^{2\pi}\int_0^{2\pi}\int_0^{\pi}\int_0^{2\pi} p_X[\varphi,\ \vartheta,\ \psi, f(t);\ \rho,\ v,\ e]d\varphi$$

$$\times \sin\vartheta\, d\vartheta d\psi\, \frac{dt}{df}\, df\, , \qquad (3.1)$$

where P is the initial orbital period of the binary. See § IIc for the transformations between true anomaly f and time t.

Finally the cross section is the effective surface area for process X to occur, defined by

$$\sigma_X(v, e) = 2\pi\int_0^\infty P_X(\rho, v, e)\rho d\rho\ . \qquad (3.2)$$

To determine the numerical value of σ_X, the theoretical definition (3.2) can be approximated by

$$\sigma_X(v, e) = \pi\rho_{max}^2(v, e)\frac{n_X(v, e)}{n_{tot}(v, e)}\ . \qquad (3.3)$$

Here $n_X(v, e)$ and $n_{tot}(v, e)$ are the number of individual scattering experiments for which the outcome X has taken place, and the total number of experiments, respectively, in a given velocity band for given eccentricity. Equation (3.3) is valid only for a specific distribution of initial conditions, which is taken to be random according to the weight factor in the integrand of equation (3.1) (cf. § IIc).

The expressions in equation (3.2) and (3.3) are *total* cross sections, with parameters depending only on the initial conditions of the scattering orbits. To obtain information about the distribution with respect to a variable characterizing the situation after scattering has taken place, we have to use *differential* cross sections with respect to that variable. This will be illustrated in § IVd.

c) Error Discussion

Numerical orbit integration from initial conditions obtained in Monte Carlo fashion leads to two kinds of errors in the determination of cross sections. First of all there is the statistical uncertainty inherent in all Monte Carlo calculations:

$$\Delta_{stat}\sigma_X(v, e) = [n_X(v, e)]^{-1/2}\sigma_X(v, e)\ . \qquad (3.4)$$

The second error source is due to limitations in both numerical accuracy and computer time. Of these, the numerical errors can be kept sufficiently small by choosing small enough integration steps. As discussed in § IIb, the maximum variation in the total energy was

not allowed to grow beyond 1% in absolute value for each individual orbit. The numerical errors leading to variations in conserved quantities are highly dependent on the particular parameters of an orbit. Therefore, the net relative error in an averaged quantity such as a cross section is much smaller than the maximum errors occurring in one orbit. Thus the final *systematic* errors due to numerical inaccuracies are estimated to be much less than 1% for the cross sections of interest. For comparison, a 1% accuracy with respect to *statistical* fluctuations in a certain (e, v) range would require 10^4 outcomes of type X in that range, or a total number of experiments considerably larger.

More serious is the limitation on computer time. In each run there are always a few unfortunate choices of initial conditions for which a disproportionately large amount of integration steps would be required to determine the outcome of the scattering experiment. This might be caused by a near triple collision which produces a large stretching of fictitious time or could be the result of the formation of a new binary with a very elongated orbit. In the latter case the third particle has to proceed to a great distance before it is clear whether the new binary is really bound, and we have a necessary stretching of real time (see Fig. 3). This last case does not pose a real problem for the purpose of the present paper, where we do not investigate the details of resonance scattering (which will be reported in a future publication).

This contribution to the error from the limitation on computer time is not statistical, since it only happens under special circumstances. We therefore have to consider the systematic error

$$\Delta_{sys}\,\sigma_X(v, e) = \pi\rho_{max}^2(v, e)\frac{n_{und}(v, e)}{n_{tot}(v, e)}\ , \qquad (3.5)$$

where n_{und} denotes the number of undetermined cases for which orbit integrations are discontinued after exceeding a prescribed bound on the number of integration steps. Since it is difficult to get a theoretical estimate of this type of error, all integrations have been done with a generous upper bound on the computing time per individual orbit (this is doubly necessary since a larger number of integration steps requires a larger accuracy *per step* in order to comply with the final 1% maximum energy error requirement, which by itself requires smaller integration steps and thus an even larger total number). In all runs we have allowed a maximum number of integration steps of a few times 10,000, while a typical orbit requires only a few hundred integration steps.

Because these critical cases do not occur frequently, total computation time is only increased by 20%–30%, when compared to imposing a much tighter time constraint. We have been able in this way to reduce the number of undecided cases to less than one in 1000. Therefore, for all practical purposes this error is irrelevant in the determination of the cross sections reported below. For completeness we did include,

however, this systematic contribution to the errors in the data reduction leading to the total cross sections.

In Appendix B the total error is determined, taking into account the statistical fluctuations not only in the number of X outcomes but also in the number of outcomes determined to be not X. Also included is a refinement of equation (3.3) to correct for undefined outcomes, where $\Delta_{sys}\sigma_X(v, e)$ is treated on the same level as a 2 σ statistical uncertainty. This might well be too pessimistic, but we feel that it is better to be careful in the present situation where little is known *a priori*.

For a 1 σ confidence level the true σ_X^{true} is expected to be in the range

$$\sigma_X^{exp} + \Delta_- \sigma_X < \sigma_X^{true} < \sigma_X^{exp} + \Delta_+ \sigma_X ,$$

where σ_X^{exp} denotes the experimentally determined value. The results from Appendix B can be summarized as

$$\sigma_X^{exp} = \pi\rho_{max}^2 \frac{n_X}{n_{tot} - n_{und}} , \qquad (3.6)$$

$$\Delta_+ \sigma_X = \frac{\pi\rho_{max}^2}{n_{tot} - n_{und}}$$
$$\times \left[n_X \frac{(n_{tot} - n_{und} - n_X)}{n_{tot} - n_{und}} + \frac{n_{und}^2}{4n_{tot}^2} (n_{tot} - n_{und} - n_X)^2 \right]^{1/2} , \qquad (3.7)$$

$$\Delta_- \sigma_X = \frac{\pi\rho_{max}^2}{n_{tot} - n_{und}}$$
$$\times \left[n_X \frac{(n_{tot} - n_{und} - n_X)}{n_{tot} - n_{und}} + \frac{n_{und}^2}{4n_{tot}^2} n_X^2 \right]^{1/2} . \qquad (3.8)$$

Note that the final combined error is asymmetric.

d) The Topological Structure of Phase Space

To obtain more insight in the details of the full underlying dependence on all nine irreducible parameters, some orbit calculations were performed for parameter values on a three-dimensional grid while keeping the other six parameters fixed. The restrictions were chosen by limiting all orbits to one plane, starting with an initially circular binary orbit, and taking all masses equal. That left as free parameters only the incoming velocity, the impact parameter, and initial orbital phase angle of the binary. Taking a grid with 6 velocity values, 40 impact parameter values, and 72 phase angle values, nearly 10,000 scattering experiments were performed (a factor of 2 was gained by symmetry with respect to exchange of the two identical binary members).

As expected, a wealth of sensitive dependence on individual parameters was visible. Looking in this way at the topology of the scattering process through an effective microscope, three-body phase space showed a complicated landscape of isolated islands in between multiply-branching rivers. Several overall features were readily identified. As an example, an incoming field star in a corotating grazing orbit was able to ionize or exchange at far larger impact parameters than a field star in a retrograde orbit. Especially at lower incoming velocities prograde orbits were able to set up wide resonances in maximum impact parameter values for specific orbital phases, whereas retrograde scattering was much less phase dependent. While these features served as an extra initial test of the whole numerical procedure, they remain interesting in themselves as probes of the underlying structure of three-body phase space. These investigations will be further discussed in a separate paper (Hut 1983b).

IV. RESULTS

Results for the total cross sections are presented in Figures 5–8. The statistics are most accurate for circular initial binary orbits, as is clear from the small 1 σ error bars in Figure 5, where the result of half a million experiments are plotted. It is striking that the process of averaging over angles has smoothed out all small scale features. The same is true for Figure 6, which summarizes 250,000 experiments at initial orbital eccentricity 0.7, and Figure 7, from 50,000 experiments at the extreme eccentricity value 0.99.

The lack of dependence on eccentricity in the cross sections is remarkable. At high velocity this can be expected, since analytic approximations of close two-body encounters lead to cross sections dependent mainly on the semimajor axis of the binary (in leading order the eccentricity dependence drops out after averaging over different binary orbital phases). These approximations, plotted in Figure 5–8, are derived in Paper II (Hut 1983a). But also at intermediate velocity values there is little eccentricity dependence: less than 20% for both ionization and exchange.

Resonance is somewhat more affected: enhancements of up to 50% occur for high eccentricity, as compared to circular orbits. This is understandable since the time-averaged separation of the two stars is larger for high eccentricity, resulting in a higher range of three-body capture.

In Figure 8 an additional 9000 circular orbit experiments are presented. The cross sections for exchange plotted here are determined as the sum of direct exchanges, which are observed in the numerical experiments, and indirect exchanges, which are estimated to occur at two-thirds of the rate of resonance cases, assuming that all three stars have the same probability to escape. The smooth transition in Figure 8 between the ranges where resonance and direct exchange dominate adds strength to this assumption. Future experiments are planned to test this hypothesis thoroughly.

a) Ionization

Ionization is possible only for positive total energy. After ionization, all stars become unbound and carry off kinetic energy in different directions. Just above threshold, where the incoming velocity $v \equiv v_3/v_c = 1$,
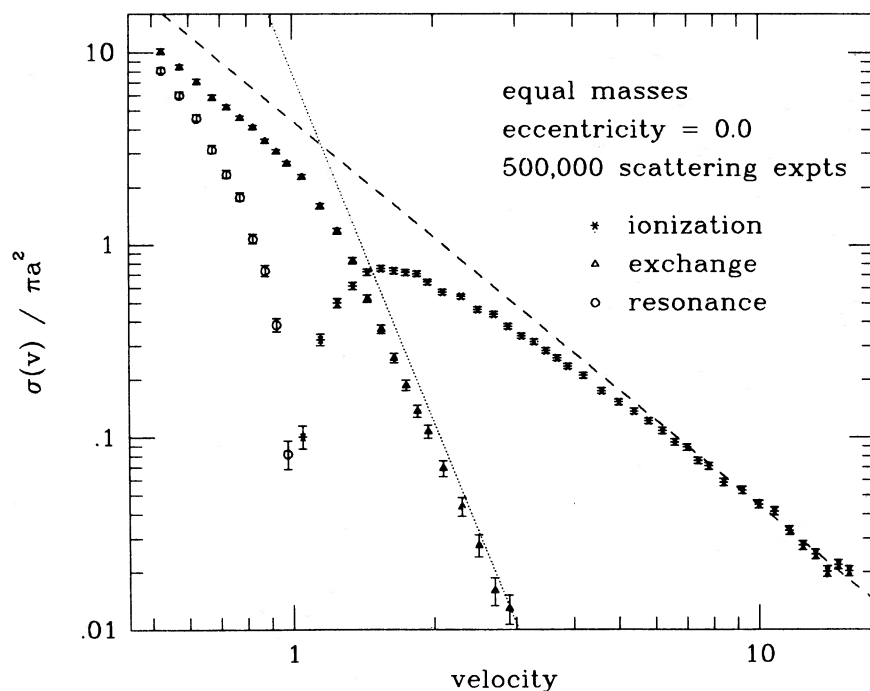
FIG. 5.—Total cross sections for an originally circular binary orbit in units of πa^2, where a is the semimajor axis of the initial binary orbit, versus incoming velocity of the single star in units of v_c, the velocity at threshold (where the total energy of the whole system is zero). The dashed line is the high-velocity analytical approximation for ionization (eq. [4.1]), and the dotted line for exchange (eq. [4.2]). Here and in all subsequent figures the following notation is used: vertical error bars are at the 1 σ level, while the indicated cross sections are obtained as averaged values over adjacent velocity bins; resonance scattering is defined as a scattering process where $s(t)$ (eq. [2.7]) has more than one minimum; For $v < 1$, the number of exchanges is estimated as the sum of the number of direct exchanges and two-thirds that of the resonances.
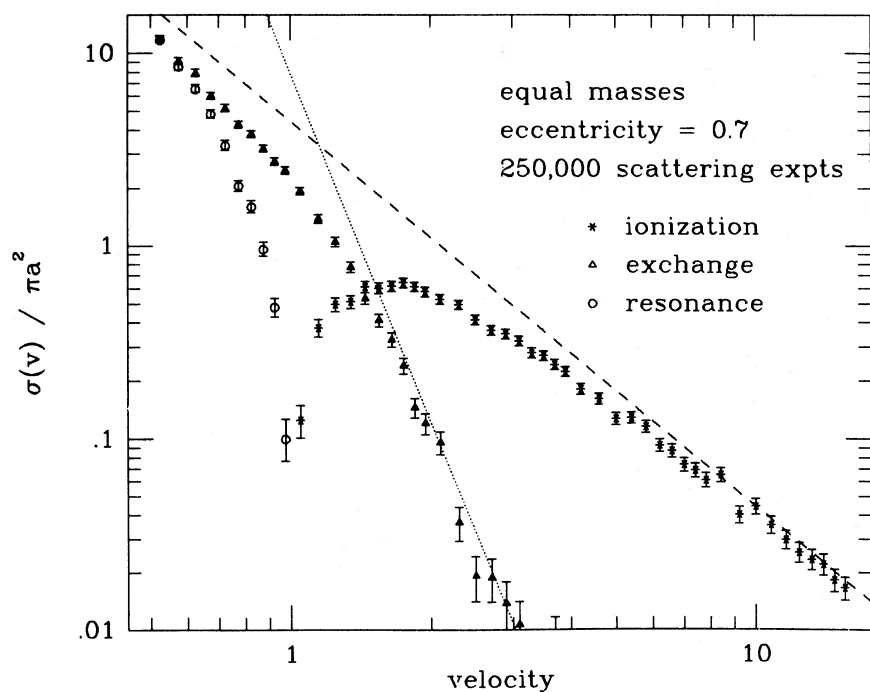

FIG. 6.—Total cross sections as in Fig. 5, but for original binary orbital eccentricity 0.7
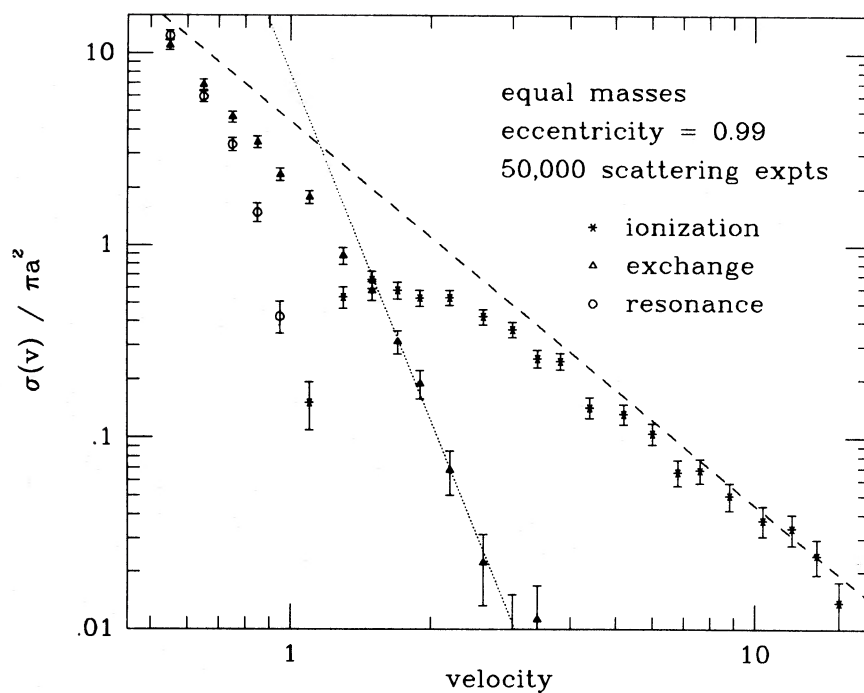
330

FIG. 7.—Total cross sections as in Fig. 5, but for original binary orbital eccentricity 0.99
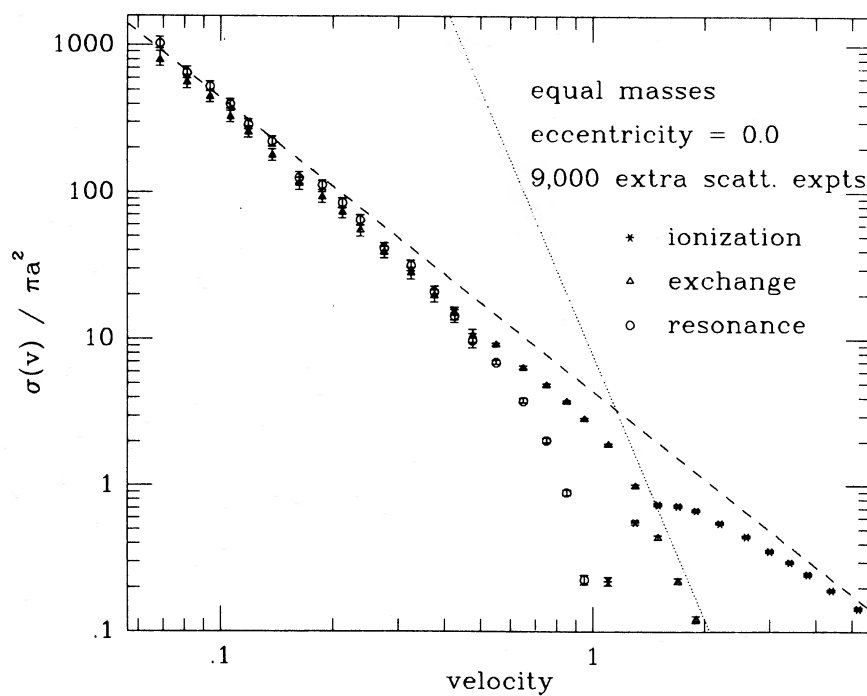

FIG. 8.—Total cross sections for an originally circular binary orbit as in Fig. 5, but for small incoming velocity

331

the ionization cross section is small because little phase space is available for the decay products. For higher incoming velocity, $\sigma_{ion}(v, e)$ rises steeply as more phase space becomes available to a value of order of the geometric cross section, $\sigma_{ion}(v, e) \sim \pi a^2$.

In the limit of high v, ionization is possible only when the incoming star passes close enough to one of the binary stars to impart sufficient momentum during the short encounter. Since this distance must be much shorter than the semimajor axis, $\sigma_{ion}(v, e)$ is much smaller than the geometric cross section and falls off rapidly with v. In the impulsive approximation, where we neglect the orbital motion during the encounter, we can determine the cross section for scattering with each of the binary members. To leading order in v this can be treated as a two-body hyperbolic encounter. The full expressions for the differential cross sections in this approximation are given in Paper II, equation (3.22). Integrating the expression for all changes in binding energy $\Delta < -1$ gives equation (5.1) of Paper II, which in the equal-mass case reduces to

$$\sigma_{ion}(v, e) = \frac{40}{9} \pi a^2 \frac{1}{v^2}, \qquad (4.1)$$

independent of eccentricity.

b) Exchange

For large field star velocities we can again use the impulsive approximation to estimate the cross section for exchange of the field star for one of the original binary members. To leading order in the small quantity v_1/v_3, the only contribution comes from knock-on collisions where the field star makes a nearly 180° turn around a binary member, which must have the same mass as the field star (Shakeshaft and Spruch 1979). In this case nearly all the incoming momentum is transferred to that binary member and, if the collision is central enough, the field star will remain bound to the other star of the original binary. At higher incoming velocities the window for large angle deflection becomes smaller *and* the tolerance for deviations from 180° scattering becomes more stringent. This results in a steep drop of the exchange scattering cross section $\sigma_{ex}(v, e)$ with increasing v.

The cross section for exchange scattering is derived in the impulsive approximation in Paper II, equation (5.2). The result is

$$\sigma_{ex}(v, e) = \frac{640}{81} \pi a^2 \frac{1}{v^6}, \qquad (4.2)$$

again independent of eccentricity.

For $v < 1$, we estimate the total number of exchanges as the sum of the number of direct exchanges and two-thirds of that of the resonances. The accuracy of this assumption depends on the degree to which resonance scattering mixes the stars. In a future paper we will present complete (but very time consuming) orbit

calculations of resonance scattering, which will enable us to determine all scattering cross sections accurately for $v < 1$.

c) Resonance

Resonance scattering is the most difficult of all gravitational scattering processes to treat analytically. The dependence on incoming velocity is mainly determined by gravitational focusing, which becomes important for low velocity, and which gives $\sigma \propto v^{-2}$ with a proportionality constant of order of the geometric cross section. To go beyond this result requires a detailed analysis, which we postpone to a future publication where we will present more specific low-energy results, such as differential cross sections. Here we give only total resonance cross sections, which agree well with the expected dependence: $a^2 v^{-2}$. In fact, in Figure 8 an increase can be seen in the cross section in addition to the gravitational focusing effect. This increase is related to an extra logarithmic factor in v, as discussed in Heggie (1975a).

d) Differential Cross Sections

More detailed information about flyby and exchange situations is presented in Figures 9–12, where the binding energy of the binary after scattering is compared with the original binary binding energy. Differential cross sections are plotted for the relative energy change,

$$\Delta = \frac{E_{bin}(t \to +\infty) - E_{bin}(t \to -\infty)}{E_{bin}(t \to -\infty)}, \qquad (4.3)$$

where *bin* stands for binary binding energy, and differential cross sections are defined in the usual way: the expression

$$\int_{\Delta_1}^{\Delta_2} \frac{d\sigma}{d\Delta} d\Delta$$

denotes the total cross section for the binary binding energy to change an amount Δ in the range $\Delta_1 < \Delta < \Delta_2$. The error bars in Figures 9–12 indicate the statistical contribution only, since we have no information about the distribution of undecided cases over the different Δ-bins (v in Figs. 5–8 is a variable which is fixed as an initial condition, whereas Δ can be determined only after a successful orbit integration).

Differential cross sections for binding energy increase (decrease) are indicated with circles (stars) in Figures 9–12. A relative binding energy decrease greater than unity would indicate ionization, and is not plotted here (whenever ionization was established, orbit integration was halted, and no detailed energy information on the single stars was obtained). Each figure displays four plots for different incoming velocity. The velocities indicated are median values, the measurements extending over a band of velocities, minimally 10% lower and maximally 20% higher than the median value.

The eccentricity dependence is much stronger for small energy exchange than in the total cross sections for ionization and exchange, as can be seen in Figures 9–11.
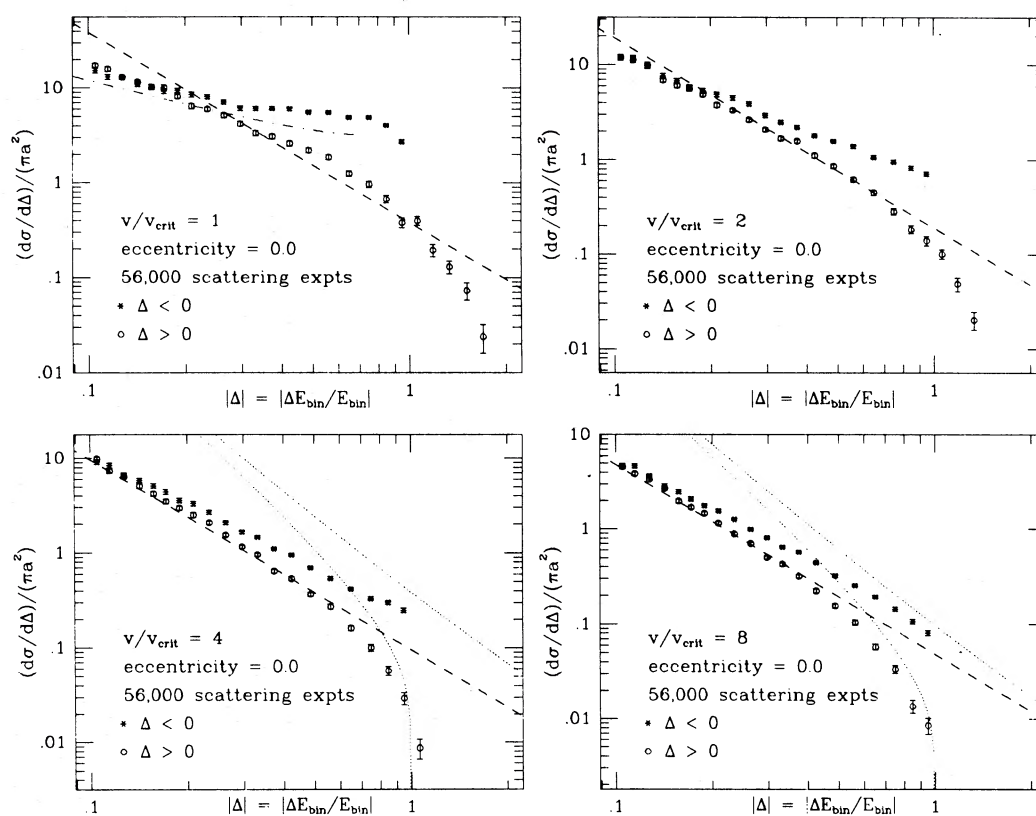
Fig. 9.—Differential cross sections for changes in binding energy, for originally circular binary orbits. Both flyby and exchange cases are added here, as well as in the following two figures. Here and in the next three figures the following notation is used: The dotted lines indicate the analytical estimates in the two-body impulsive approximation; the dashed lines are for the tidal impulsive approximation; and the dashed-dotted line indicates the orbitally averaged tidal approximation.

In the upper left-hand plots there is an increase by a factor 3 in $d\sigma/d\Delta$ going from $e = 0$ to $e = 0.99$. For very large increases of binary binding energy, $\Delta > 1$, there is an even more marked difference. Here the cross section drops off much steeper for lower eccentricity. As one might have expected, it is easier to obtain a very tight orbit by deforming a very eccentric orbit than by starting with a circular orbit.

In the upper left-hand plots in Figures 9–11, the incoming velocity is centered around threshold ($v = 1$; $E_{tot} = 0$). Here the shape of the starred curve ($\Delta < 0$) differs from that at higher velocities by an increase in the form of a shoulder at intermediate values, which is followed by a dip in the differential cross section at $\Delta = -1$. The dip is just a threshold phenomenon, arising from phase-space limitations, since nearly all the kinetic energy of the incoming star has to be used to widen the binary close to ionization. The shoulder results from the superposition of flyby and exchange cases, as is shown in Figure 12. Of course, it is only for equal-mass situations that it is reasonable to add these two different processes; for unequal stellar masses, binaries of different mass would be formed.

In case of exchange, no singularity is present at $\Delta = 0$ in Figure 12, but a dip occurs just below $\Delta = -1$.

This lowered value of $d\sigma/d\Delta$ is again the result of phase space limitations: here nearly all kinetic energy has to be neutralized to create the new, very wide binary. This leaves little room in velocity space for such final states, and consequently their production is suppressed.

In the simplest case of three-body scattering the incoming star leaves the original binary intact and changes only the binding energy and angular momentum. The differential cross sections for changes in binary energy during such a "flyby" scattering are derived in the impulsive approximation of two-body scattering (neglecting the interaction with the third star during a close encounter) in Paper II, and are plotted in Figures 9–11 as dotted lines. Note the strong dependence on eccentricity for $\Delta > 1$.

The two-body impulsive approximation is excellent for large energy changes at high incoming velocity, such as are required for ionization and exchange scattering. However, very small energy changes in flyby scattering generally result when the incoming star does not come near one of the binary members. The two-body approximation does not apply in this case. A better alternative is to consider the tidal gravitational field of the passing star and its influence on the binary orbit. For high enough incoming velocity, the impulsive
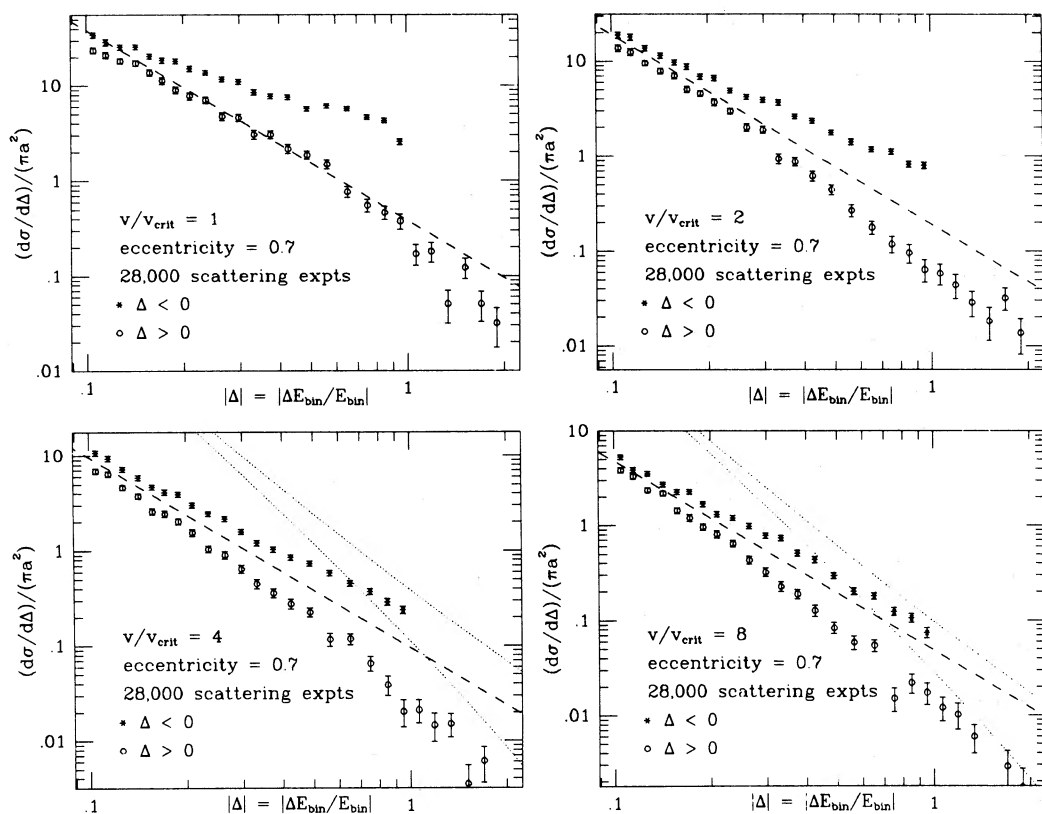
FIG. 10.—Differential cross sections for changes in binding energy, for original binary orbital eccentricity 0.7
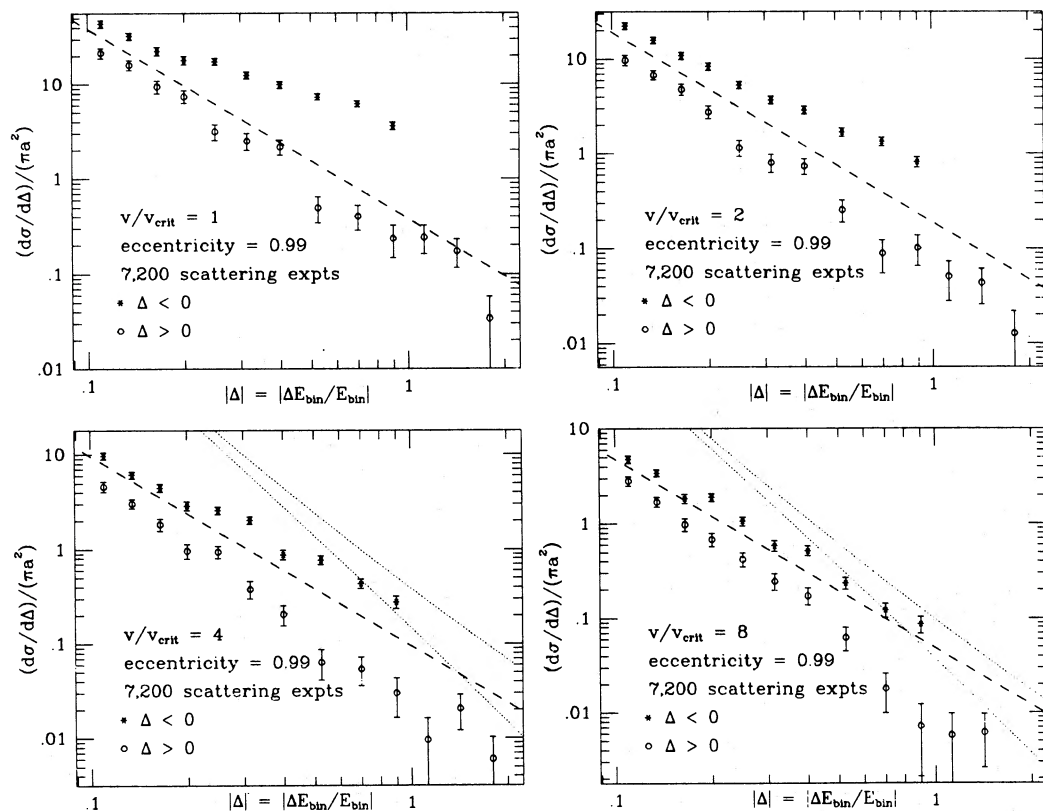
FIG. 11.—Differential cross sections for changes in binding energy, for original binary orbital eccentricity 0.99
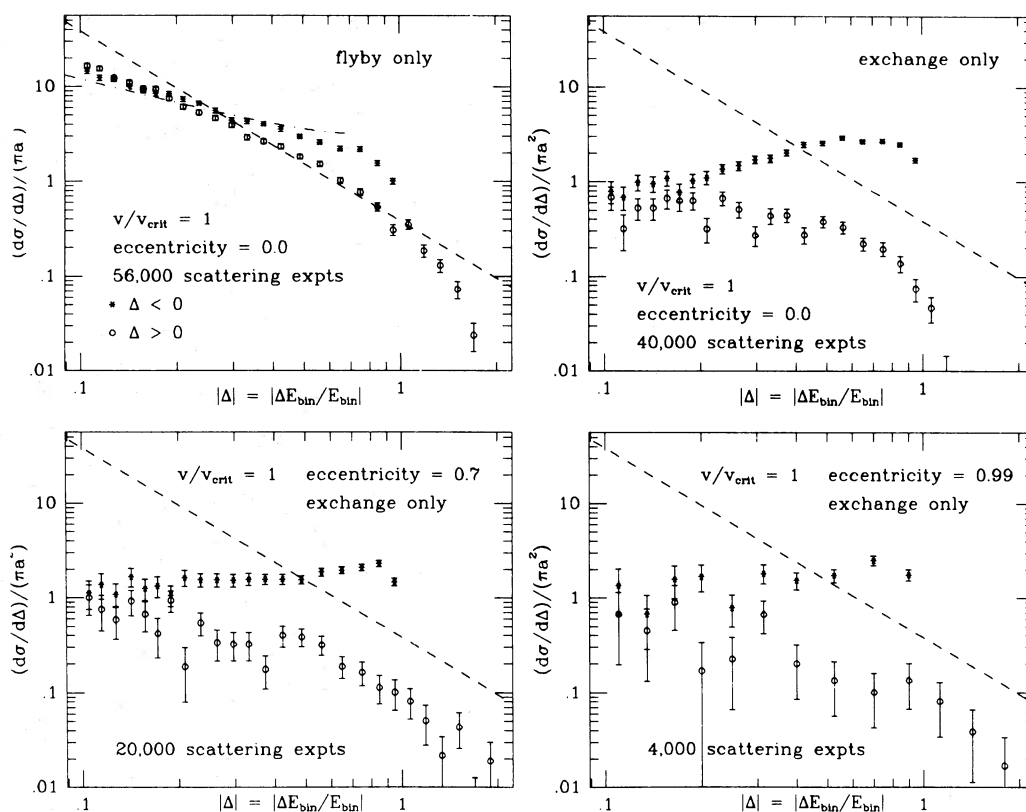
FIG. 12.—Differential cross sections for changes in binding energy, divided according to flyby and exchange

approximation can still be used, and the result, as given by Heggie (1975a) in the limit of small Δ, is:

$$\frac{d\sigma}{d\Delta}(\Delta; v, e) = \frac{2}{3^{3/2}}\pi a^2 \frac{1}{v}\frac{1}{\Delta^2}. \qquad (4.4)$$

This result holds both for positive and negative Δ in leading order in $1/\Delta$; the difference between the two is itself of order $1/\Delta$, and thus much smaller, in accord with detailed balance, the differential cross section being slightly larger for negative Δ (soft binaries tend to become softer).

If Δ is further decreased while keeping the incoming velocity fixed, we encounter situations where the impulsive approximation also breaks down. Here we can no longer neglect the orbital motion of the binary during the scattering, which complicates the analysis considerably. This situation becomes especially important at low incoming velocities, and we will defer a discussion to a future paper which will deal especially with scattering for states of negative total energy. In Figure 12 we show a formula given by Heggie (1975a):

$$\frac{d\sigma}{d\Delta}(\Delta; v, e) = 2^{2/3}\pi a^2 \frac{1}{v^2}\frac{1}{|\Delta|}\left(\frac{-1}{\ln|\Delta|}\right)^{1/3}. \qquad (4.5)$$

Strictly speaking, this expression is expected to apply only to hard binaries, but it turns out to give a reasonable result even for the intermediate case of $v = 1$.

V. THERMAL AVERAGES: RATE FUNCTIONS

a) Formalism

In this section we discuss how we obtain thermal averages of the scattering cross sections via parameter fitting and integration over a Maxwellian spectrum of field star velocities. We illustrate the method by computing thermal averages for ionization, a process for which we have a complete set of data, since it occurs only for $v > 1$.

In a spatially homogeneous field of equal mass stars the thermal distribution function of their velocities can be approximated by a Maxwellian:

$$f(v) = \left(\frac{2}{\pi}\right)^{1/2}\left(\frac{m}{kT}\right)^{3/2}\exp\left(-\frac{\frac{1}{2}mv^2}{kT}\right)v^2 dv, \qquad (5.1)$$

as long as we make the usually justified approximation of neglecting deviations of the high-energy tail which arise from stars escaping from the system under consideration.

Note that $v \equiv v_3/v_c$ is dimensionless, and therefore $T \equiv T_{\text{phys}}/v_c^2$, where T_{phys} is the real temperature in physical units. Further on in this section we will change to the variable v_{th}, the average thermal velocity, which also is dimensionless.

Binaries formed from these equal mass stars have a combined mass $2m$, and a thermal distribution function

$$f'(v) = \left(\frac{2}{\pi}\right)^{1/2} \left(\frac{2m}{kT'}\right)^{3/2} \exp\left(-\frac{mv^2}{kT'}\right) v^2 dv , \quad (5.2)$$

where $T' = T$ in the case of equipartition of translational energy, and $T' = 2T$ if the binaries have the same velocity dispersion as single stars. Depending on their formation and subsequent history, a realistic T' for binaries lies somewhere between these extremes.

In the instantaneous rest frame of a binary the distribution of relative velocities of single stars is again given by a Maxwellian, but now with an effective mass m^* and temperature T^*:

$$m^* = \frac{m2m}{m + 2m} = \frac{2}{3} m ;$$

$$T^* = \frac{m^*}{m} T + \frac{m^*}{2m} T' = \frac{2}{3} T + \frac{1}{3} T' . \quad (5.3)$$

We thus have for the relative velocities

$$f^*(v) = \left(\frac{2}{\pi}\right)^{1/2} \left(\frac{m^*}{kT^*}\right)^{3/2} \exp\left(-\frac{\frac{1}{2}m^*v^2}{kT^*}\right) v^2 dv , \quad (5.4)$$

where from now on we will characterize the temperature T^* by the thermal velocity dispersion in the *relative* velocities:

$$v_{\text{th}}^2 \equiv \langle v^2 \rangle_{f^*} = 3(kT^*/m^*) . \quad (5.5)$$

The thermally averaged rate for a typical binary to undergo a particular scattering with cross section $\sigma(v)$ is given by

$$n \langle v\sigma(v) \rangle_{f^*} ,$$

where n is the density of field stars, here assumed to be homogeneous. In the following we will use the dimensionless quantity

$$R(v_{\text{th}}) \equiv \frac{\langle v\sigma(v) \rangle_{f^*}}{\pi a^2 v_{\text{th}}} , \quad (5.6)$$

which will be of order of the scattering cross section in units of the geometrical cross section at the thermal velocity.

b) Ionization: Parameter Fitting

The most convenient way to derive the average ionization rate is by integration over a thermal distribution of a cross section curve derived from the numerical experiments by parameter fitting. There are two constraints on the shape of the function to be fitted. At threshold ($v = 1$) the function has to vanish, and for high field star velocities it has to approach the analytic expression, given in equation (4.1).

We have constructed a trial function by starting with the high-energy analytic approximation, and adding higher order terms in $1/v$. The number of free parameters is then always one lower than the number of added terms, because of the requirement that the cross section vanish at threshold. A drawback in this

method is that the dependence on v is forced to be linear just above threshold. However, inspection of the data shows a very steep rise at threshold, making the detailed behavior there relatively unimportant since this region contributes only a rather small amount to the thermal average (unless $v_{\text{th}} \ll 1$).

This relative unimportance of threshold phenomena is illustrated by the case of circular binary orbits, for which 10,000 scattering experiments in the range $1 < v < 1.1$ established a power law dependence roughly as $\sigma \propto (v - 1)^{1.3}$. However, the total number of ionizations which were observed in this velocity region, 52 out of 10,000, is rather small. Therefore the power law fit with a power 1.3 indicates that a linear approximation just above threshold introduces only very small errors in the overall fit.

Good accuracy can be obtained with a one-parameter fit. The deviations can be made less than 10% over most of the velocity range, for all eccentricities for which our scattering data are sufficiently accurate to constrain the parameters. However, at the low-energy side of the peak in the cross section, the fit could not be made very satisfactorily, leaving deviations in this region of up to 50%. Combining the best fits for different eccentricity values, we have found the best overall fit to be

$$\sigma(v, e) = \frac{40}{9} \pi a^2 \frac{1}{v^2} \left(1 + \frac{-0.75 - 0.4e}{v} + \frac{-0.25 + 0.4e}{v^2}\right) . \quad (5.7)$$

A two-parameter fit gives much better results, achieving a 10% accuracy almost everywhere except just above threshold. For our purpose of deriving thermal rate functions with an accuracy of 10% this is good enough. Again, combining the best fits for individual eccentricity values, we have found the best overall fit to be

$$\sigma(v, e) = \frac{40}{9} \pi a^2 \frac{1}{v^2}$$

$$\times \left(1 + \frac{-0.2 - e}{v} + \frac{-1.8 + 2e}{v^2} + \frac{1 - e}{v^3}\right) . \quad (5.8)$$

To establish this fit we have used data obtained for nine different eccentricities (see § IIIa).

c) Ionization Rates

Using the two-parameter fit obtained above, it is straightforward to integrate $v\sigma$ over a thermal distribution. The result is

$$R(v_{\text{th}}, e)$$

$$= \frac{40}{3} \left(\frac{2}{3\pi}\right)^{1/2} \left[1 + (1 - e) \frac{3}{v_{\text{th}}^2}\right] \frac{1}{v_{\text{th}}^2} \exp\left(-\frac{3}{2v_{\text{th}}^2}\right)$$

$$- \frac{40}{3} \left[\frac{1}{5} + e + (1 - e) \frac{3}{v_{\text{th}}^2}\right] \frac{1}{v_{\text{th}}^3} \text{erfc} \left(\frac{3}{2v_{\text{th}}^2}\right)^{1/2}$$

$$+ 40 \left(\frac{2}{3\pi}\right)^{1/2} \left(-\frac{9}{10} + e\right) \frac{1}{v_{\text{th}}^4} E_1 \left(\frac{3}{2v_{\text{th}}^2}\right) , \quad (5.9)$$

where the complement of the error function and the first exponential integral are defined by (Abramowitz and Stegun 1972);

$$\text{erfc } z \equiv 1 - \text{erf } z = \frac{2}{\pi^{1/2}} \int_z^\infty e^{-t^2} dt \; ; \quad E_1(z) = \int_z^\infty \frac{e^{-t}}{t} dt \; .$$

The rate function $R(v_{th}, e)$ is plotted in Figure 13. The dashed line indicates the high temperature ("Rayleigh-Jeans") limit, which can be obtained as the leading term in an expansion of the rate function in $1/v_{th}$:

$$R(v_{th}, e) = \frac{40}{9} \left(\frac{6}{\pi} \right)^{1/2} \frac{1}{v_{th}^2} + O(v_{th}^{-3}) \; . \quad (5.10)$$

The low temperature ("Wien") limit shows an exponential dropoff, as the leading term in an expansion in v:

$$R(v_{th}, e) = \frac{32}{27} \left(\frac{6}{\pi} \right)^{1/2} \exp \left(-\frac{3}{2v_{th}^2} \right) + O(v_{th}^2) \; . \quad (5.11)$$

The ionization rate, according to $R(v_{th}, e)$ as given in equation (5.9) and plotted in Figure 13, is estimated to be correct to within 10% at the 3 σ level for all $v_{th} \geq 1$. For $v_{th} \gg 1$ the accuracy becomes progressively better, since analytic approximations are more reliable. For $v_{th} < 1$, deviations might be slightly larger than 10%, since the ionization rate at low v_{th} is mainly determined by a very small part of the low-energy tail of the ionization cross section, so that any error there will be amplified considerably.

It is clear from Figure 13 that the eccentricity dependence of the ionization rate is rather weak. This can also be seen from the two limiting expressions (5.10) and (5.11), where the eccentricity has dropped out in leading order. However, the slight decrease in the ionization rate for increasing eccentricity is a real effect, as can be checked by direct inspection of the cross section curves (Figs. 5, 6).

For practical purposes the full expression (5.9) for the rate function can be approximated by a smooth transition between the two limiting expressions (5.10) and (5.11):

$$R_{approx}(v_{th}) = \frac{32}{27} \left(\frac{6}{\pi} \right)^{1/2} \frac{1}{1 + (2/15)v_{th}^2}$$
$$\times \left[1 + \exp \left(\frac{3}{2v_{th}^2} \right) \right]^{-1} \; . \quad (5.12)$$

This approximation is eccentricity independent, since both limiting expressions contain no eccentricity dependence. It turns out to be rather accurate: the deviation from the full expression for circular orbits is nowhere larger than 10%. For all eccentricities the deviations are bounded by:

$$-0.1 < \frac{R_{approx}(v_{th}) - R(v_{th}, e)}{R_{approx}(v_{th})} < +0.2 \; .$$

VI. DISCUSSION

The main improvement of the present work over previous publications is made possible by the much larger number of integrations we have been able to do. We have reported results from 1.7 million orbit calculations, an order of magnitude more than the
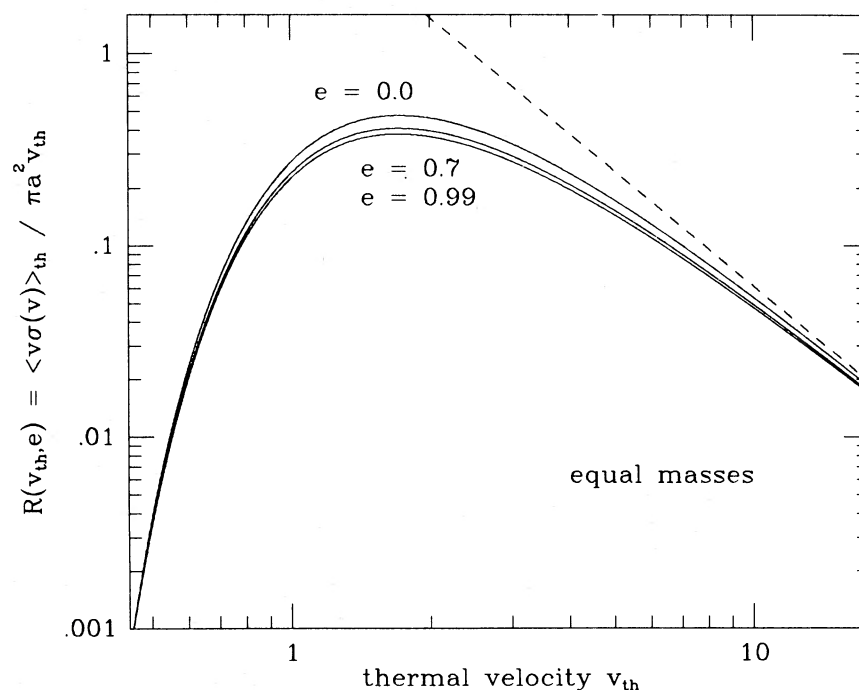

FIG. 13.—The rate function for ionization as a function of thermal velocity v_{th} in dimensionless units, for three eccentricity values

combined number in all previous investigations. This increase in the number of orbit calculations has enabled us to present for the first time cross sections computed by a Monte Carlo sampling of the whole of phase space without any *a priori* assumptions about the dependence on angles or impact parameter. The present paper deals exclusively with equal-mass stars and is the first in a series in which a representative coverage will be attempted of general binary–single star scattering.

The result for the total cross sections of ionization, exchange, and resonance scattering, as well as for differential cross sections with respect to energy exchange, are plotted in Figures 5–12 in § IV. The differential cross sections, measuring the degree of inelasticity of binary–single star scattering, are given for positive total energy; a more detailed treatment of resonance scattering will be given in a later publication.

The thermal ionization rate was determined by fitting the cross sections (in § V) to a simple expression for the dependence of ionization upon field star velocity and binary orbital eccentricity. This expression was integrated analytically over a Maxwellian spectrum of field star energies. The resulting expression for the ionization rate was approximated by a simple interpolation formula, equation (5.12), accurate to 10 % (20 %) for initially circular (eccentric) binary orbits and arbitrary thermal velocity.

Two main features are apparent in all the cross section curves discussed here: the surprising success of simple analytic approximations (many due originally to Heggie), and the relative insensitivity to the orbital eccentricity of the original binary. Both ionization and exchange scattering follow the analytic predictions for high field star velocities, in the impulsive two-body approximation, down to velocities not much above the critical velocity. In general, all cross sections we have calculated, total as well as differential, exhibit smooth turnovers between different domains of analytic approximation, with little unexpected behavior. The explanation for the tameness of these features must lie in the extreme effectiveness with which the averaging over the four configuration angles and the impact parameter manages to wash out all irregular behavior. The underlying, microscopic structure of three-body phase space is extremely sensitive to small changes in system parameters, as discussed in § III*d*.

All the cases considered here are relatively insensitive to the initial orbital eccentricity of the binary. Whereas cross sections change over many orders of magnitude as a function of binary semimajor axis and incoming field star velocity, the dependence on eccentricity generally amounts to less than a factor 2, and often is even much weaker. The reason for the different behavior may be caused by the fact that a and v determine the internal and external energy of the three-body system, whereas eccentricity is connected with internal angular momentum (dependence on external angular momentum is washed out by integration over different impact parameters).

This insensitivity on eccentricity is of great practical advantage. It allows one to treat e as a redundant variable by averaging over an appropriate spectrum, e.g., the thermal equilibrium distribution $f(e) \propto e$. Using the results of this paper, and the assumption of thermal equilibrium, upper limits can be derived for the maximum error appropriate to a particular application. The relative insensitivity to eccentricity is the main reason that we did not present here separate differential cross sections with respect to energy *and* eccentricity exchange.

In conclusion we mention the great practical value of the many analytical approximations given by Heggie (1975*a*). Many of the features in the cross section curves which survive the fivefold averaging over angles and impact parameter were readily understandable from his analysis, both qualitatively and quantitatively. To explain some other features, such as the dependence on eccentricity of the differential cross sections at high energy exchange values, and details of exchange scattering, additional analytic approximations are presented in Paper II.

APPENDIX A

AUTOMATIC TERMINATION OF NUMERICAL INTEGRATION

The outcome of a scattering experiment can take three different forms, as described in § II*d*, depending on the formation of a bound three-body system, a bound two-body system, or the complete disruption of the whole system. The first type mentioned, resonance, occurs only for negative total energy and will ultimately decay into the second type. This second type can be either a flyby or exchange, and occurs both for positive and negative total energy values. The third type, ionization, only occurs for positive total energy.

Following the entire evolution of the slowly decaying three-body configuration in case of resonance scattering would take a very large amount of computer time, because the outcome is sensitive to slight variations in the initial conditions. Therefore numerical integration was generally halted after a few pulsations of such a configuration.

To run many thousands of experiments requires a fully automatic test procedure to determine at which point numerical integration should be stopped. This test subroutine must be able to predict when the switch can be made,

within a given accuracy, to the analytic two-body approximation. It also must recognize which of the three types of outcome outlined above has taken place.

To avoid wasting computing time, a test procedure was applied only after the point of closest triple approach was reached. A convenient measure is the mean square distance, defined in equation (2.7):

$$s(t) = \left[\tfrac{1}{3} \sum_{i<j} |r_i(t) - r_j(t)|^2 \right]^{1/2} , \qquad (A1)$$

which can be small only when all three stars are close together. At the beginning of a numerical integration, $s(t)$ monotonically decreases. After $s(t)$ passes through its first minimum, the test procedure is applied once after every 20 integration steps.

The test subroutine is made up of four different checking routines. First of all, numerical accuracy is tested by determing the change in the total energy, which is a conserved quantity. In § IIb it is explained how a large error causes a rerun of the whole calculation with increased precision.

A second check utilizes the mean square distance. In most cases $s(t)$ passes through only one minimum. When several minima occur, the computation is automatically halted, since multiple minima are a clear signature of a resonance process. As a halting criterion, the occurrence of four minima in $s(t)$ was used in most cases.

A third check is to determine whether ionization has already occurred. Care has to be taken to evaluate the correct three-body energy. Even when each pair of stars is unbound when treated as three two-body problems, the interference of the third star can cause one pair to converge together and form a new double star. However, it is straightforward to find lower limits that guarantee ionization when imposed simultaneously on the positive relative energy of each pair of stars.

As a fourth step, every pair of stars is tested as a possible candidate for forming a new binary. If the separation of two stars is at least a factor 3 smaller than the smallest distance between each of them and the third star, a further test is made to determine whether the third particle will actually escape to infinity. Lower bounds on the required energy can be given just as in the ionization case. However, in the case where a binary is left behind, numerical integration is continued even if escape is established. The energy and eccentricity of the binary are calculated, typically to 1% of the original binary energy and 0.01 in the eccentricity.

Fortunately, this requirement of high numerical accuracy does not lengthen the calculation too much: the uncertainty in the energy of the escaping star can remain much bigger than 1%. The reason is that subsequent energy exchange takes place mainly between the single star and the center-of-mass motion of the binary. The coupling between the single star and the internal motion of the binary occurs via tidal forces, falling off rapidly with distance.

If none of the four previous tests have stopped the calculation, another 20 integration steps are undertaken. In between each integration step only two operations are performed: computation of the size of the next time step and a check for occurrence of a new minimum in the mean square distance, $s(t)$.

Of course, there is always the possibility that after a long time no signal to stop is obtained. This generally occurs in two cases. At every value of the incoming velocity, there is a slight chance that two or three stars approach each other so closely that the regularized time step size nearly drops to zero. This can increase the number of integration steps to an unacceptable limit, and therefore an upper limit is imposed on the total number of integration steps. The upper limit can be fairly high, even of the order of 10,000. The reason is that only very few orbits come so near to collision that this limit is actually achieved, and the total fraction of computing time spent on these critical orbits is still small. It turns out that with an upper limit of 10,000 steps less than one out of 10,000 experiments remain undecided.

The second, and more serious, case for which computation time gets out of hand arises only at low incoming velocity, when resonances occur, i.e., only for negative total energy. Whenever one star moves away from the other two in a very elongated ellipse, it can taken an arbitrarily long time before the isolated star has completed one full orbit and three-body interaction becomes an essential factor again. In the present version of the program, no allowance is made as yet to treat these and similar cases as a separate class. This is of course possible, by supplementing the full three-body numerical computation with separate two-body approximations, which can be calculated using analytical expressions. This procedure is already applied in every orbit to determine the initial conditions at the start of the numerical integration (see § IIb).

APPENDIX B

ERROR ANALYSIS

There are two types of errors contributing to the final uncertainty in the cross sections, as discussed in § IIIc. Here we present a detailed description of the adopted total error, treating systematic errors on the same level as 2 σ statistical errors.

The cross section $\sigma(v, e; m_2, m_3)$ for the outcome of a scattering experiment to be of type X, is an average probability, obtained by an integration over the four orientation angles and the impact parameter. We consider a large number of scattering experiments for fixed mass ratios, initial binary orbital eccentricity, and a narrow range of incoming velocities, the width of which we will ignore. In the following we suppress the functional dependence on these remaining four independent scattering variables.

We assume that the initial conditions are distributed in parameter space according to the appropriate weight factor, given in equations (3.1)–(3.2), as will be the case in a homogeneous and isotropic medium of field stars. Other distributions will lead to more complicated expressions, the derivation of which is completely analogous.

The total number of scattering experiments n_{tot} can be divided by n_X, the number of experiments with an outcome of type X; n_{oth}, the number of times that the outcome is determined not to be of type X; and n_{und}, the (small) number of experiments of which the outcome is not defined because the integration was halted after exceeding the time limit. Obviously

$$n_{\text{tot}} = n_X + n_{\text{oth}} + n_{\text{und}} \ .$$

The best estimate for the cross section, without any *a priori* knowledge of the nature of the undecided orbits, is obtained by simply discarding those orbits. This leads to a refinement of equation (3.3):

$$\sigma_X{}^{\text{exp}} = \pi d_{\text{max}}^2 \ \frac{n_X}{n_X + n_{\text{oth}}} \ , \tag{B1}$$

where ρ_{max} is the maximum value of the range of impact parameters used in the scattering experiments.

The statistical error, inherent in any Monte Carlo approach, is proportional to the square root of the number of hits *and* the square root of the number of misses. The second contribution is important only in situations with a small number of misses, and leads to a refinement of equation (3.4):

$$\Delta_{\text{stat}} \sigma_X = \sigma_X \left(\frac{1}{n_X}\right)^{1/2} \left(\frac{n_{\text{oth}}}{n_X + n_{\text{oth}}}\right)^{1/2} \ ,$$

or more symmetrically

$$\Delta_{\text{stat}} \sigma_X = \pi d_{\text{max}}{}^2 \ \frac{1}{(n_X + n_{\text{oth}})^{1/2}} \left(\frac{n_X}{n_X + n_{\text{oth}}} \frac{n_{\text{oth}}}{n_X + n_{\text{oth}}}\right)^{1/2} \ . \tag{B2}$$

For very small values of n_X or n_{oth} this expression should be replaced by the appropriate Poisson distribution. However, for all practical purposes considered here, the estimate given in equation (B2) is accurate enough.

The systematic error arising from unidentified experiments cannot be estimated reliably without any further knowledge about their distribution and characteristics. However, it is possible to give firm upper and lower limits to their contribution to σ_X. The largest possible change is the increase of the true cross section with respect to the experimentally determined value, in the case that *all* the undecided experiments have the characteristic X. This is indicated in equation (3.5) and, with the correction from equation (B1), leads to

$$\sigma_X{}^{\text{true}} < \sigma_X{}^{\text{exp}} + \Delta_{\text{stat}}{}^+ \sigma_X = \pi \rho_{\text{max}}^2 \ \frac{n_X + n_{\text{und}}}{n_{\text{tot}}} \ , \tag{B3}$$

which is strictly valid for $n_{\text{tot}} \to \infty$, where $\Delta_{\text{stat}} \sigma_X \to 0$.

The lower limit to the systematic correction results in a smaller deviation, in the case that *none* of the undecided experiments are of type X. We thus have

$$\sigma_X{}^{\text{true}} > \sigma_X{}^{\text{exp}} - \Delta_{\text{stat}}{}^- \sigma_X = \pi \rho_{\text{max}}^2 \ \frac{n_X}{n_{\text{tot}}} \ , \tag{B4}$$

again for $n_{\text{tot}} \to \infty$.

The rather conservative combined 1σ error estimates, equations (3.7)–(3.8), result from the sum of the squares of statistical and systematic errors, where we treat the maximum possible systematical error as an equivalent 2σ statistical error.

REFERENCES

Abramowitz, M., and Stegun, A. 1972, *Handbook of Mathematical Functions* (New York: Dover).
Alekseev, V. M. 1981, *Amer. Math. Soc. Transl.* (2), **116**, 97 Ninth Math. Summer School (Kaciveli, 1971) [transl. of *Izdanie Inst. Mat. Akad. Nauk Ukrain. SSR*, Kiev, 1972, pp. 212–341].
Batten, A. H. 1973, *Binary and Multiple Systems of Stars* (Oxford: Pergamon).

Fabian, A. C., Pringle, J. E., and Rees, M. J. 1975, *M.N.R.A.S.*, **172**, 15p.
Fullerton, L. W., and Hills, J. G. 1982, *A.J.*, **87**, 175.
Heggie, D. C. 1975a, *M.N.R.A.S.*, **173**, 729.
———. 1975b, in *IAU Symposium 69, Dynamics of Stellar Systems*, ed. A. Hayli (Dordrecht: Reidel), p. 73.
———. 1977, *Rev. Mex. Astr. Ap.*, **3**, 169.

Heggie, D. C. 1980, in *Globular Clusters*, ed. D. Hanes and B. Madore (Cambridge: Cambridge University Press), p. 281.
Hills, J. G. 1975, *A.J.*, **80**, 809.
Hills, J. G., and Fullerton, L. W. 1980, *A.J.*, **85**, 1281.
Hut, P. 1983a, *Ap. J.*, **268**, 342 (Paper II).
———. 1983b, *The Topology of Three-Body Scattering*, preprint.
Monaghan, J. J. 1976a, *M.N.R.A.S.*, **176**, 63.
———. 1976b, *M.N.R.A.S.*, **177**, 583.
———. 1977, *M.N.R.A.S.*, **179**, 31.
Nash, P. E., and Monaghan, J. J. 1978, *M.N.R.A.S.*, **184**, 119.
Olson, R. E., and Salop, A. 1977, *Phys. Rev.*, **A16**, 531.
Percival, I. C., and Richards, D. 1975, in *Advances in Atomic and Molecular Physics*, ed. D. R. Bates and B. Bederson (New York: Academic), Vol. **11**, p. 1.
Press, W. H., and Teukolsky, S. A. 1977, *Ap. J.*, **213**, 183.
Saslaw, W. C., Valtonen, M. J., and Aarseth, S. J. 1974, *Ap. J.*, **190**, 253.
Shakeshaft, R., and Spruch, L. 1979, *Rev. Mod. Phys.*, **51**, 369.
Siegel, C. L., and Moser, J. K. 1971, *Lectures on Celestial Mechanics* (New York: Springer).
Valtonen, M. J., and Aarseth, S. J. 1977, *Rev. Mex. Astr. Ap.*, **3**, 163.
Valtonen, M. J., and Heggie, D. C. 1979, *Celest. Mech.*, **19**, 53.
Zahn, J.-P. 1977, *Astr. Ap.*, **57**, 383.

PIET HUT and JOHN N. BAHCALL: Institute for Advanced Study, Princeton, NJ 08540